SOFTWARE AND AUTOMATION SESSION SUMMARY

Chairs: Werner Gurtner and Jan McGarry

Automation continues to increase throughout the ILRS Network as can be seen in the presentations by Pearson on Mt Stromlo, Pierron on FTLRS, and Xin on TROS. Automation calls for more and more complicated software. Matt Pearson showed that software of the future needs to be modular, loosely coupled, flexible and reusable.

Automation improvements occur in both the hardware and software. Hardware enhancements were presented by Degnan on the SLR2000 beam expander, Wang on new control systems for San Juan, and the use of FPGAs in SLR systems digital design at Beijing by Li and at TROS by Xin.

Chris Moore demonstrated in his presentation that an automated system can perform as well as a manually operated system by giving statistics for Mt Stromlo when it was fully automated and when it was manually controlled.

Werner Gurtner showed that other work can share the telescope system in an automated way with SLR at no performance loss, given the right software to control the system.

New tools and formats are helping SLR stations in their transition to new technologies and in capturing these changes as they happen. This was seen in the presentations by Salminsh on web applications for engineering, and on the Consolidated Prediction and Consolidated Data Formats by Ricklefs.

The presentation by Heiner and Schreiber showed how to improve automated real-time signal processing by reprocessing (looking behind and projecting ahead) which can provide a 10–40% improvement over normal histogram analysis.

Progress in automation, reliability, performance and maintainability continues to be made at stations across the ILRS. Each group has their own approach to improvements. Sharing of these different technical approaches is the most important part of the Workshops.

A Comparison of Performance Statistics for Manual and Automated Operations at Mt Stromlo

C.J. Moore[1]

1. EOS Space Systems Pty. Limited, 111 Canberra Ave., Griffith, A.C.T. Australia.

Contact: cmoore@eos-aus.com

Abstract

The new Mt Stromlo SLR Station was rebuilt in the 12 months following the destruction of the original station by the January 2003 bushfires, and was reopened in April 2004. It became fully operational in December 2004 and since then the station has been operated manually pending completion of the development of a more advanced infra-structure that will support automated operations.

The original station had conducted automated operations for over three years before the bushfires and the performance measures that were in place during this period have continued to be collected for recent operations. This provides a unique opportunity to compare the productivity performance between automated and manual operations undertaken at the same site and with the same management team.

Provided that periods of abnormal events are taken into account, net productivity from these two modes of operation are quite comparable with differences less than about 5% over periods of many months. The fact that automated operations persist for longer periods and in conditions that discourage manual operation appear to compensate for the efficiencies that human interaction can provide.

Introduction

The original Mount Stromlo SLR Station (7849, STRL) was commissioned in Oct 1998, and subsequently performed automated operations from late 1999 until being totally destroyed in the January 2003 Canberra bushfires. A more complete description of the operation of this station has been given by Luck, Moore and Greene (2000). During this period, operations included the automated download of predictions, tracking of satellite and calibration targets, data processing and upload of published data. Automated operations allowed the station to continue operations, collecting and publishing SLR data, while it was unmanned. In fact, such operations were effectively unmanned for 80% of the time.

Productivity metrics were captured for this whole period. As described in Luck et al, these metrics were used for establishing performance criteria required under the contract between EOS and AUSLIG (subsequently incorporated into Geoscience Australia). Processing of productivity data and generation of reports was only partially automated, with a significant component requiring routine, but brief human inspection and assessment of the system and environment.

Subsequent to the 2003 bushfires, the remains of the old station were removed and the new Mount Stromlo SLR Station (7825, STL3) was constructed on the same site. All systems were functional by the official opening in April 2004, less than 14 months later. After undergoing stringent testing of all of the new sub-systems, including a new software system and completing formal acceptance testing, the new station commenced full operations in December 2004. Given the rapid redevelopment of the station, the system (in 2005-2006) was not capable of automation hence the station has been operated manually in a more traditional manner using operators rostered to

cover day and night, seven days a week. The new station was only unmanned when lack of targets or poor weather precluded productive tracking. It should be noted however, that contractual requirements (as well as good practice) required continuing capture of productivity metrics and generation of performance reports. The definition and processing of these data had not changed between the automated and manual operations.

The availability of reasonable long time series in these two data sets, has therefore allowed the relative performance between automated and manual SLR operations to be assessed. It should be remembered that the two stations were both designed by EOS and operated by EOS staff and hence have much in common. It was considered that the physical and technical differences between the two stations did not influence productivity levels to such an extent as data quality and other factors.

Metrics

The metrics used in this assessment include the following;

1. The number of all ILRS satellite passes with a maximum elevation above the 20 degree site horizon.
2. The number of all possible passes – i.e. the number of passes that are trackable, accounting for poor weather, low elevation passes and pass overlaps or priority.
3. The number of attempted passes – i.e. the number of possible passes for which the SLR station fired the laser in an attempt to track the satellite.
4. The number of passes that were successfully tracked – i.e. at least one normal point was generated.

The following figure shows the time series of these metrics for the two periods.

Figure 1: Productivity Metrics

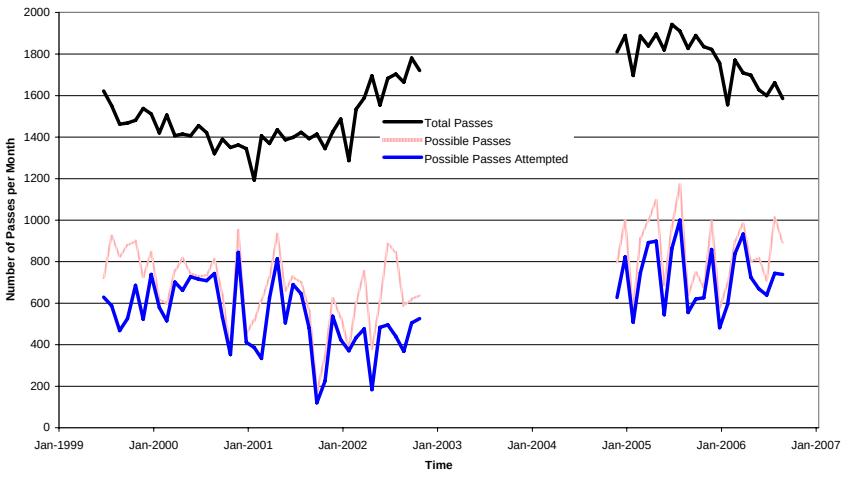

Results

Potential Productivity

Figure 2 provides the number of passes successfully tracked normalized by the number of possible passes. This ratio provides a measure of the system's potential productivity. If the ratio reached 100% then every pass that could realistically be tracked would be tracked. This figure shows that on average the potential productivity of the automated system reached 66% while than manned system was significantly more successful with an average potential productivity of 74%. Note that some exceptional points were excluded from the calculation. The points were associated

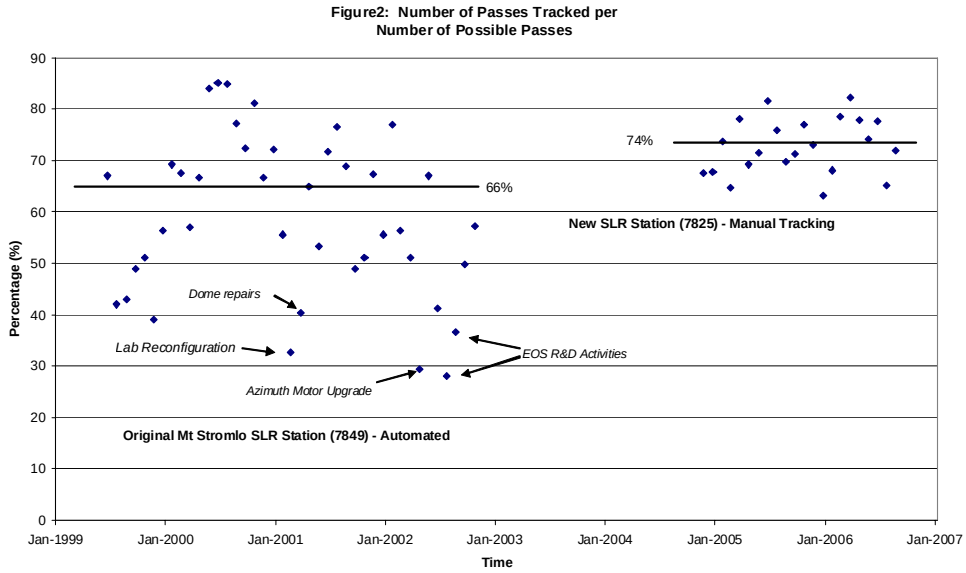

with station activities that significantly affected the ability of the station to perform normal operations. This result suggests that everything else being equal, a human operator should outperform a mechanical system, where for example a human can respond to unusual events such as system failures more quickly.

Tracking Capability

The next figure provides the number of passes successfully tracked normalized by the number of attempted passes. This ratio provides a measure of the system's capability for successfully tracking a target. If the ratio reached 100% then every pass tracked would result in generation of normal points. Figure 3 shows that on average the potential productivity of the automated system was 81% while the manned system was marginally more successful with an average of 87%. Note that a few exceptional points were again excluded from the calculation. For example, at one point the telescope enclosure was slipping due to a mechanical fault such that the system continued to attempt passes, but a misalignment of the telescope and dome meant that no returns were possible.

These results suggest that as long as a pass is attempted, the automated system has on average as nearly as good a chance in successfully acquiring the target as a human operator. Perhaps any skills that an operator may have in acquiring a target is balanced by the persistence of an automated system

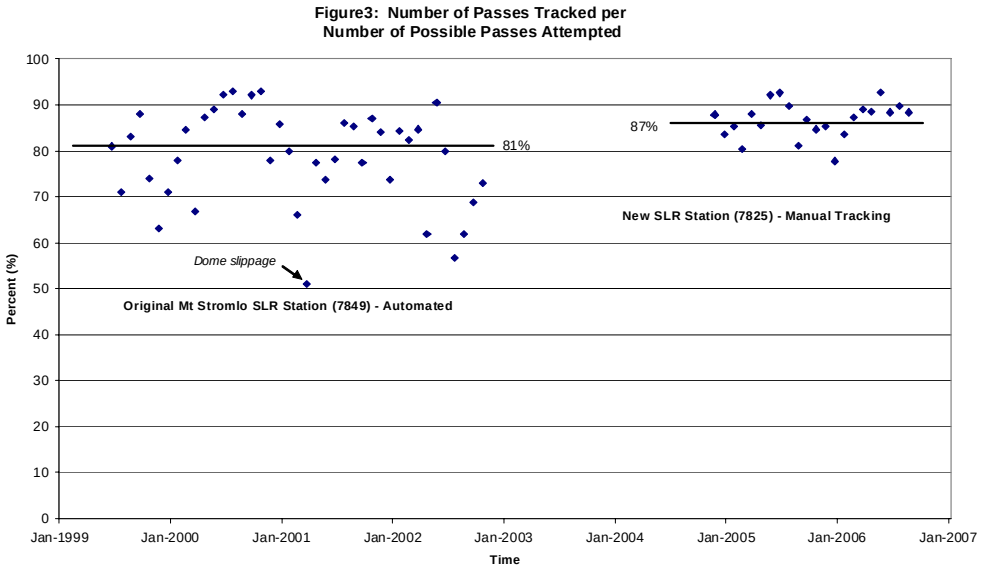

Actual productivity

The final figure provides the number of passes successfully tracked normalized by the total number of passes. This ratio provides a measure of the system's net or actual productivity, or passes tracked irrespective of conditions. In this case if the ratio reached 100% then every pass would have been tracked successfully. Figure 4 shows that on average the actual productivity of the automated system was 32% while that for the manned system was 35%, not a statistically significant difference. Note that some exceptional points were also excluded from the calculation as discussed earlier.

The major contributor to the absolute value of this ratio is of course the weather. It should be noted that during manual operations, the station was often unattended during overcast periods. In contrast, the automated system generally continued operations regardless of weather conditions. It is believed that this difference favoured the automated system, since there would have been opportunities to successful track during breaks in the sky cover or respond quickly to clearing conditions.

Conclusions

Availability of two years or more of productivity data from SLR tracking at one location, using similar techniques and equipment, and the same staff, has allowed an objective assessment of the performance from automation and manual operations.

The results indicate that there was overall very little difference in net productivity between the automated and manual operations. While human operators appear to have an advantage when on-site and undertaking tracking in clement weather, the automated system had an advantage in less ideal condition and could take opportunities that were lost to operators.

Figure 4: Number of Passes Tracked per Number of Total Passes

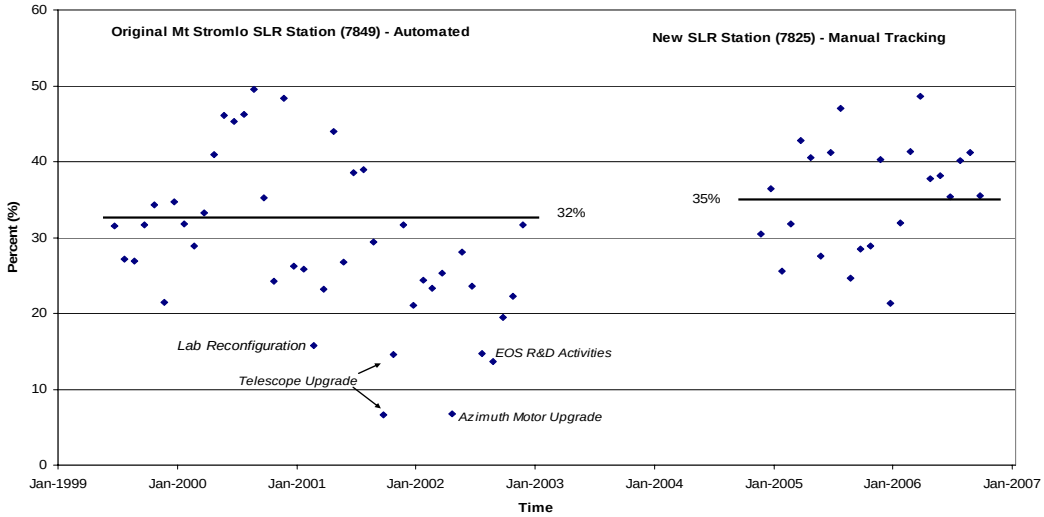

It is therefore clear that sophisticated automation systems can equal, if not better, manual operations. As far as the system at Mount Stromlo is concerned, it is felt that continuing improvements in the software and hardware systems will result in automated operations exceeding manual productivity figures.

References:

[1] Luck, J., C.J. Moore and B. Greene. Autonomous Laser Ranging Results from Mount Stromlo. Twelth International Workshop in Laser Ranging, 2000, Matera.

EOS Software Systems for Satellite Laser Ranging and General Astronomical Observatory Applications

M. Pearson[1]

1. EOS Space Systems Pty. Ltd.

Contact mpearson@eos-aus.com

Abstract

EOS has developed software systems over many years to support Satellite Laser Ranging (SLR) and the delivery of general astronomical observatories to its customers. These software systems are based upon a re-useable software architecture that simplifies systems development. The design objectives of this software architecture are discussed in the context of its evolution and current deployment at the Mt. Stromlo Satellite Laser Ranging facility, located in the Australian Capital Territory.

Introduction

This paper presents a brief overview of the software EOS has developed to support Satellite Laser Ranging at Mount Stromlo, software that has been designed to support not only SLR, but a wide range of astronomical applications.

This software, known as the 'Observatory Control System', supports EOS research and development programmes. It also supports the observatory requirements of several customers, being a flexible and scalable product, which lends itself to re-use across laser ranging and astronomical observatory applications.

Requirements

The basic requirements of the Observatory Control System are:

- it should drive equipment that might be expected at an observatory;
- it should provide some sort of abstraction – an 'Observatory' abstraction – that hides the complexity of the underlying equipment and presents it in terms that end-users and operators are likely to understand;
- it should provide facilities to automate day-to-day operations and routine observatory tasks.

Challenges

With these goals in mind, EOS has developed Observatory Control Systems over many years. But there was a problem; as the complexity of observatories grew, so did the complexity of the supporting software. This led to several challenges which are encountered in all types of software:

- it was becoming monolithic with fewer, larger, more-complex components;
- these components were highly-coupled, so changes to any part of the system could unexpectedly impact seemingly un-related parts;
- these systems were becoming inflexible and difficult to change in order to meet new requirements;
- different observatory solutions were becoming increasingly problem-specific and less re-usable; they were not amenable to solving new problems.

Solution

Under these pressures EOS engaged in a complete re-design of its software, culminating in what is now the 'Observatory Control System'.

The result is that the control system is inherently unaware of its problem domain. It is called an 'Observatory Control System' but it is in fact a generic control system. Its immediate application is to SLR and astronomy, but it could drive any automated industrial facility. It is domain independence that makes the control system highly extensible, flexible and most-importantly for EOS, re-useable.

Basic Architecture

At the highest level the Observatory Control System embodies the system concept:

'a collection of components which work together in order to solve a problem'.

These components include:

- various types of hardware and software;
- usually some sort of network;
- control system and observatory-level software.

The control system software provides facilities including:

- server frameworks;
- client frameworks;
- network interfaces.

The observatory-level software provides facilities including:

- servers;
- clients;
- automation functions.

Refer to Figure 1 for an illustration of these components.

Hardware & Software

Hardware and software include such items as: telescopes, enclosures, lasers, associated software and a variety of other equipment. A common problem with such equipment is that it is often heterogeneous, with different:

- platforms, eg. PC, Mac;
- operating systems, eg. Windows NT, XP, Linux;
- interfaces, eg. serial, CANopen, USB, Bluetooth;
- protocols, eg. sockets, CORBA, COM.

A fundamental feature of the Observatory Control System is that it makes this equipment look, feel and act in a consistent manner. This is achieved by hiding the equipment behind a universal software abstraction – what is called a Device.

Network

Devices are usually accessed through an adapter card and a driver library. But there is a limit to how many devices a given computer can support; at some point a single computer will run out of capacity, or a new device will require a different operating system or computer platform. So most observatories require many computers and the Observatory Control System is network-enabled.

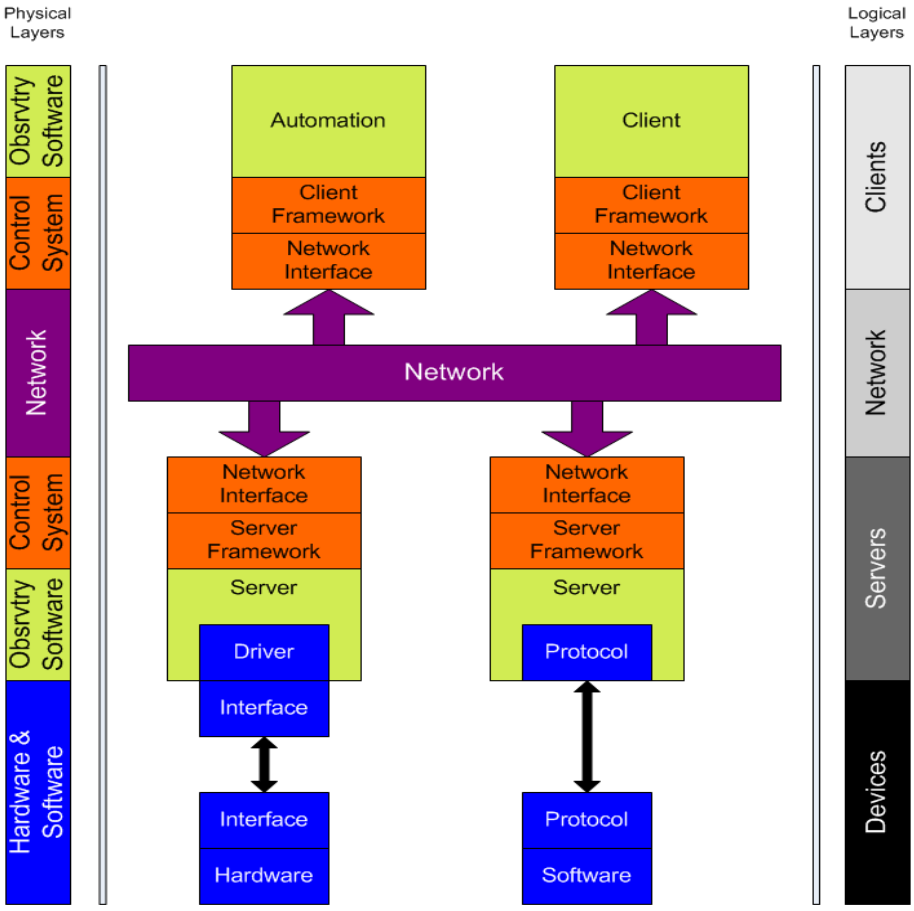

Figure 1. *Basic Software Architecture*

Control System

The Observatory Control System is a Client / Server software architecture. This is a network computing model based on the following concepts; that:

- clients connect to servers;
- clients issue commands to servers;
- servers respond to client commands.

Within the Observatory Control System, device server applications wrap devices and make them available over the network.

Client applications connect to these device servers over the network, or even over the Internet, and drive devices via commands to the relevant device server.

At the heart of the Observatory Control System are several software frameworks; these are code libraries which embody the most-re-useable, but complex and technical aspects of the control system.

These frameworks encourage re-use, and are used by EOS to extend its systems. These frameworks are also available to customers, who can extend their observatories over the longer term, independent of EOS.

Server Framework

Server applications, also known as device servers, are built using a *Server Framework*.

Servers directly manage observatory devices. A device server may manage one or many devices, depending on our requirements.

Servers may be active and/or passive; that is, they may manage devices autonomously and robotically, or in response to user commands.

Servers may participate in a hierarchy, where a parent server may depend on several child servers. Child servers provide services to their parent, which may perform some aggregate function; the parent may itself have a parent, to which it provides services, and so on.

This cooperative, 'building block' approach facilitates a separation of concerns; resulting in simple components from which complex systems can be built.

Client Framework

Client applications are built using a *Client Framework*.

Client applications are the focus of general observatory operators and users. This is where users interface with the observatory. So client applications will usually perform several functions:

- sending commands to / receiving replies from servers;
- displaying server state and responding to server state changes.

The display of server state is by a mechanism called Subscribe / Publish. The subscribing client asks for server state to be delivered at specified intervals, upon which the data is repeatedly published, arriving at the client without the need to keep asking. This asynchronous approach is much more efficient than simply polling for data. It should be noted that efficient network communications are important given the distributed, network-focused nature of the Observatory Control System.

Network Interfaces

In addition to the abstraction which hides the complexities of devices, the network provides its own abstractions – these hide the additional complexity of communicating with devices over the network. The result is that whatever the nature of a device or its location on the network, it can be accessed in a simple manner which is consistent for all devices.

All parts of the Observatory Control System employ the same, universal abstractions to facilitate end-to-end communication between client applications and the device servers which host the observatory devices.

Observatory Software

Observatory software includes client and server applications and automation applications that meet general observatory requirements and specific customer requirements. Domain and problem-specific control system functions are implemented at this level.

Like all parts of the Observatory Control System, this software is built upon a common set of software Frameworks.

It is at this level that the Observatory Control System can be customised, even by customers, with support from EOS if necessary.

Servers

Observatory-level servers will typically drive the hardware and software devices specific to any given observatory.

Clients

Client applications will provide an interface that hides the complexity of the underlying equipment, and present it in terms that end-users and operators are likely to understand.

Automation Functions

Observatory software provides system automation functions at many levels, including:

- device management – automatic management of device behaviour and state by device servers;
- scripted tasks – scripting of automation functions;
- task scheduling – scheduling of robotic tasks to be executed continuously, at scheduled intervals or in response to system events;
- closed loop control – automatic execution of system functions in response to changes in system state.

Case Study – Mount Stromlo

The Mount Stromlo facility contains two ranging systems, for satellite ranging and space debris ranging. These systems have common, but mostly different requirements, and have shared and dedicated components. But both systems were built sharing a single instance of the Observatory Control System.

This integration presented no significant problems or difficulties. Furthermore, no problems are foreseen concerning extensive capability upgrades over the next year. So the Observatory Control System provides technical certainty in terms of EOS' ability to extend and enhance its observatory systems.

Conclusion

The Observatory Control System supports EOS' demanding technical and business requirements. It has evolved over many years and continues to do so. The next evolution may well be a network of stations, where each station is a cooperating instance of the Observatory Control System. This will enable highly coordinated, world-wide observation and ranging programmes.

Currently EOS provides the Observatory Control System with its telescopes and enclosures. There is nothing inherently necessary about EOS' equipment, however; so long as basic requirements are met, the Observatory Control System can operate with any vendor's equipment. So in future EOS may offer the Observatory Control System as a stand-alone product, independent of its telescopes and enclosures.

Finally, the underlying control system is domain-independent. There are no astronomical or observatory-specific concepts embedded in the fundamental control system. So it is plausible that it could be used to drive a range of automated facilities.

Electro-Control System of San Juan SLR Station

Wang Peiyuan[1], Guo Tangyong[1], Li Xin[1], Han Yanben[2], Liu Weidong[2],
Wang Tangqiang[3], Qu Feng[3], Tan Yechun[1], Zou Tong[1]

1. Institute of Seismology, China Earthquake Administration
2. National Astronomical Observatories, Chinese Academy of Sciences
3. Chinese Academy of Surveying and Mapping (CASM)
Contact: Yangroot@yahoo.com.cn

Abstract

A new SLR station has been set up in San Juan, Argentina this year, and works well now. Since Feb. 5th, 2006 to the 4th quarter, 2006, a total of 5861 pass (include 1134 Lageos pass) was obtained[1]. Some parts of this station, including servo system, control system, control software, and some observations will be described in this paper.

Telescope Servo System

San Juan SLR station's telescope is a bi-close-loop control system, i.e. position loop and velocity loop. Angle inductosyn and tacho-generator are used for the feedback sensors. When SLR system is tracking, the DAC input is tuned by PC software to drive telescope according to the ephemeris and the telescope position. Then the PID arithmetic theory is used to figure out the PWM voltage, consulting the telescope and theoretical velocity, to drive telescope's moment motor. So using this bi-close-loop control system, the SLR system's tracking can be improved.

The mount is driven by special motion drive IC: LMD18200. Its operating voltage can be up to 55V, and operating current can be up to 3A continuous output.

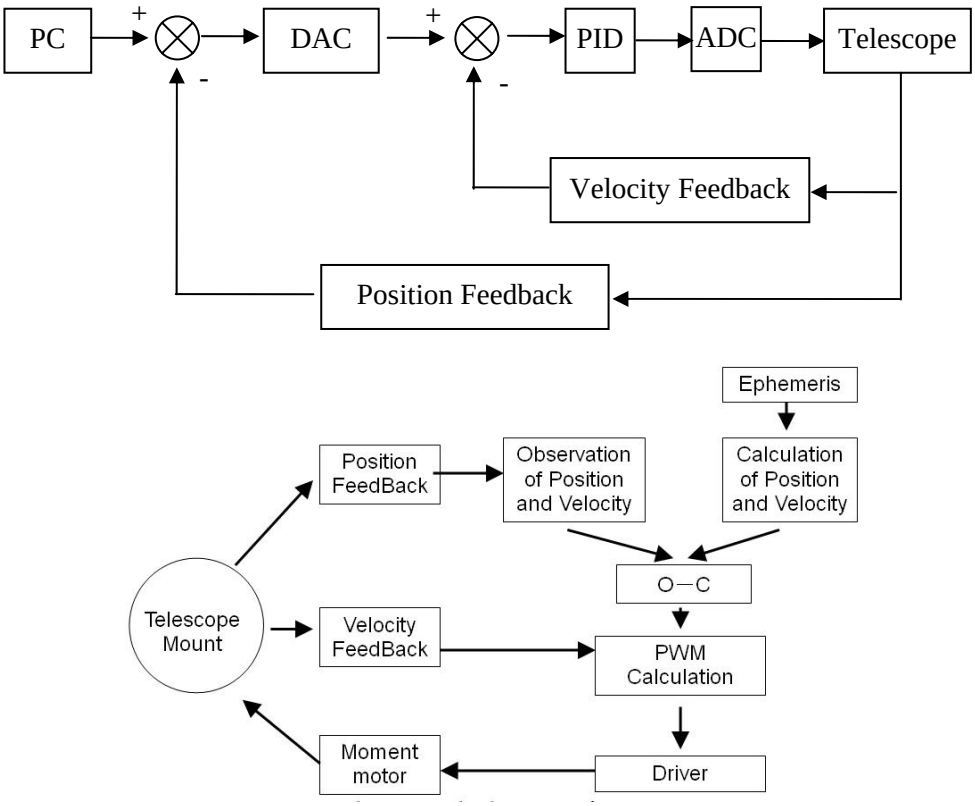

Figure 1: *the principle diagram of servo system*

Control Software

A general computer is needed to run the control software, and Figure 2 is the first picture of San Juan's tracking Lageos. Most control functions are included, such as satellite prediction, data pre-treatment, telescope servo, laser firing, range gate tuning, target measurement, data acquisition, etc.

Figure 2 is the first pass of Lageos in San Juan SLR station on Feb.5th, 2006. In this pass, 1514 samples were achieved between two green lines. The duration is about 15 minutes, and the deviation is very small (white dots).

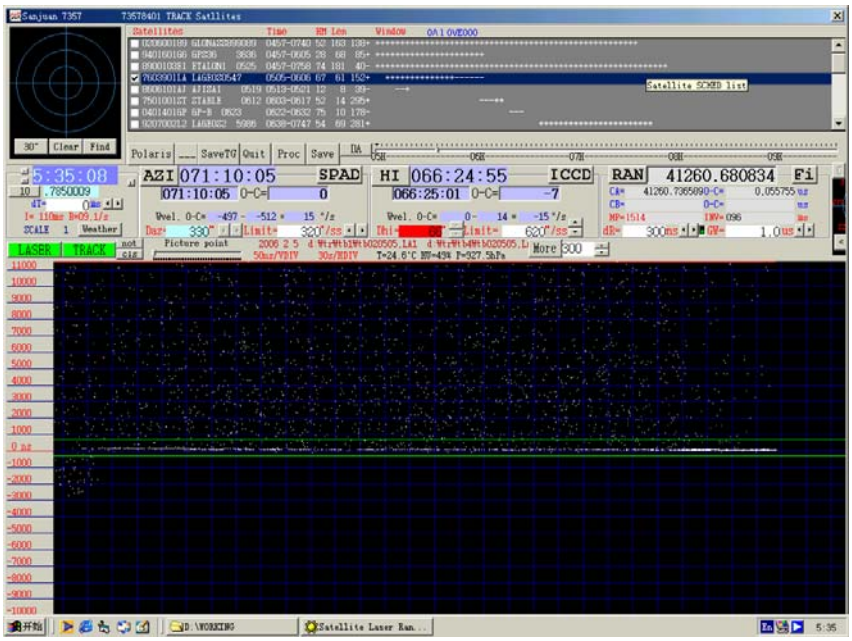

Figure 2: *Interface of control software and the first Lageos pass*

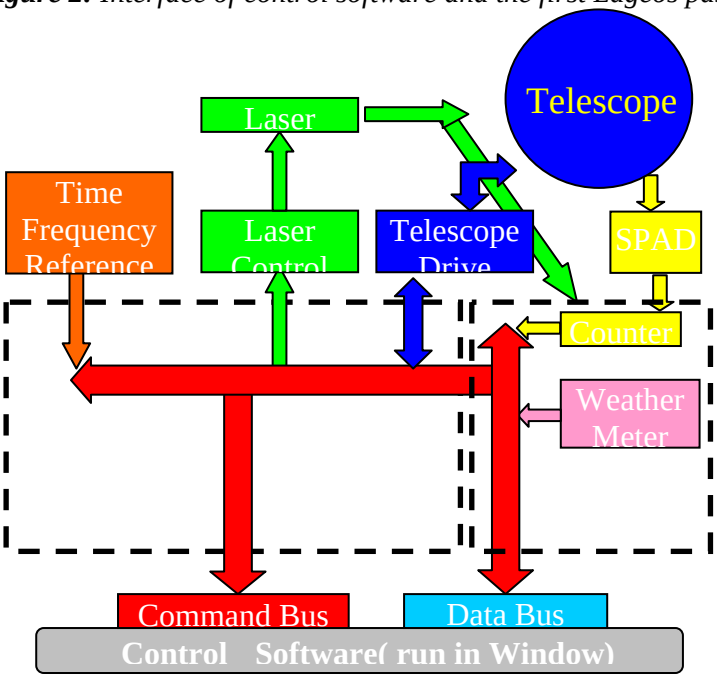

Figure 3: *The diagram of control system*

Results

The South America is lack of SLR station. The running of productive San Juan station will improve performance of the ILRS network.

Site Information		Data Volume									Data Quality		
Column 1	2	3	4	5	6	7	8	9	10	11	12	13	14
Location	Station Number	LEO pass Tot	LAGEOS pass Tot	High pass Tot	Total passes	LEO NP Total	LAGEOS NP Total	High NP Total	Total NP	Minutes of Data	Cal. RMS	Star RMS	LAG RMS
Baseline		1000	400	100	1500								
San_Juan	7406	3846	1134	881	5861	52713	13619	4180	70512	32323	6.5	10.4	12.1

Table 1: *San Juan performance report card[1]*

Reference

[1] SLR Global Performance Report Card July 1, 2005 through June 30, 2006.

[2] Wang Tangqiang, Current Status Of San Juan SLR Station In Argentina, 14th ILRS Workshop Proceedings.

[3] Guo Tangyong, The Performance and Observation of Mobile System TROS-I In China, 14th ILRS Workshop Proceedings.

Integrated Upgrades of Control System for TROS

Li Xin, Guo Tangyong, Zou Tong, Wang Peiyuan, Tan Yechun,
Xia Jiening, Zhou Yunyao, Du Ruilin

1. Institute of Seismology, China Earthquake Administration.

Contact: lxcomcn@yahoo.com.cn /Fax: +86-27-87863471

Abstract

The mobile SLR system TROS has operated for several years. Operations are routine, but the system is not without problems. To solve these problems, we are planning an upgrade to some of the TROS subsystems. These upgrades will enhance the signal return rate, improve the tracking precision and system reliability, provide convenient operational conditions for mobile observation, and relieve the labor intensive nature of the operations and maintenance.

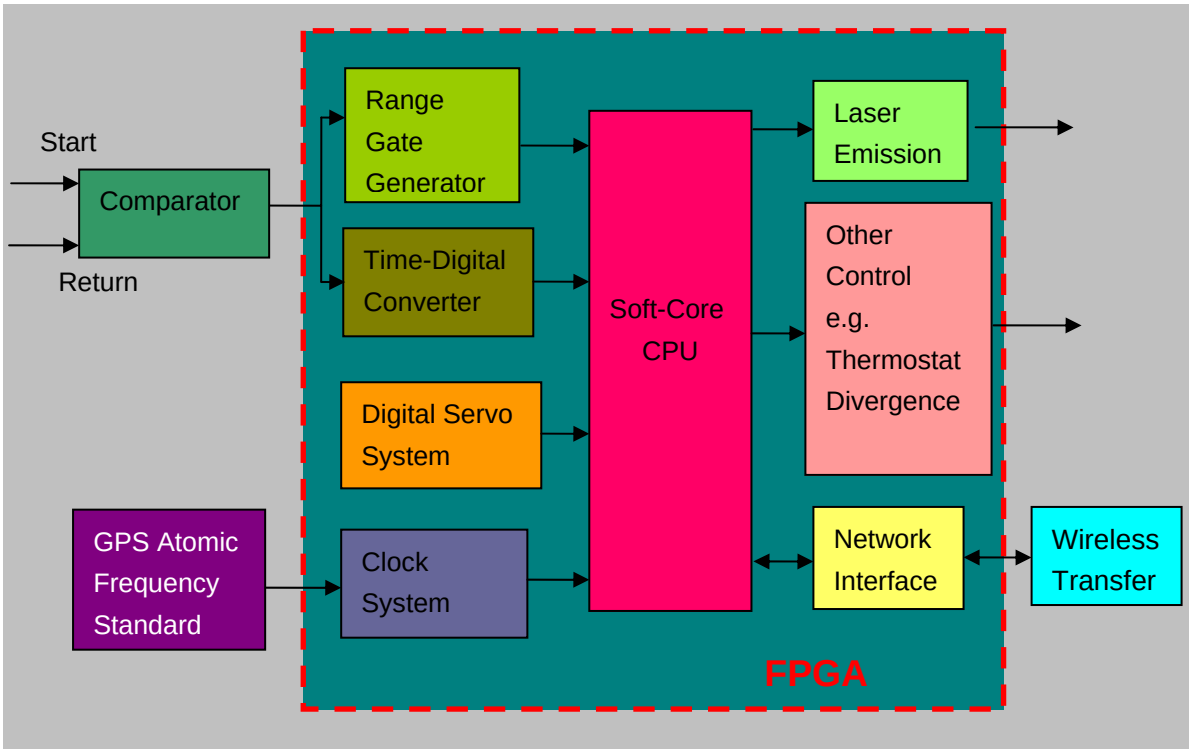

Figure 1. *The principle diagram of the control part*

The new version of TROS will possess the following properties:

1. The electronic components will be integrated into one subsystem, including event counter, GPS locked clock, range gate generator, servo system, and software. This will enhance system reliability.The principle diagram of this part is shown in Figure 1.

2. The control system will provide control for KHz ranging.This will help in target acquisition and tracking and enhance the normal point ranging precision.
3. The integrated event counter will use the time to digital converter to measure the interval in the FPGA.
4. The new electronics will generate the signal of angular position and speed by a photoelectric position encoder for implementing a full digital servo system. This will enhance tracking precision.
5. Operators will be able to run the software to control the system by web browser over wireless link.

CCD and SLR Dual-Use of the Zimmerwald Tracking System

W. Gurtner, M. Ploner

1. Astronomical Institute, University of Bern.

Contact: gurtner@aiub.unibe.ch

Abstract

The Zimmerwald Laser and Astrometric Telescope (ZIMLAT) has been designed for both satellite laser ranging and optical tracking with CCD cameras, the latter mainly for orbit determination of space debris by means of astrometric positions. The paper describes the main characteristics of the control programs, both for CCD and SLR and their interaction during interleaved operation and it summarizes some experiences after several years of dual-use.

Introduction

The Zimmerwald observatory celebrated its 50 years anniversary in 2006. Its original purpose was an astronomical observatory for the University of Bern, Switzerland, mainly designed for sky surveillance (search for supernovae, minor planets and comets). However, it developed more and more into an observatory for space geodesy, starting with optical (photographic) tracking of satellites in the sixties, laser tracking since 1976, permanent GPS (and later GLONASS) tracking since 1991 and finally optical tracking again, mainly of space debris, using CCD cameras and digital image processing. In 1997 we replaced the former SLR tracking system (50 cm telescope, Nd:YAG laser) with a new 1-meter telescope and a two-wavelength Ti:Sapphire laser (846 nm and 423 nm wavelengths). The new ZIMLAT telescope has been designed for dual use, i.e. it serves as transmitting/receiving telescope for satellite laser ranging as well as a telescope for astrometric observations of space objects, mainly space debris.

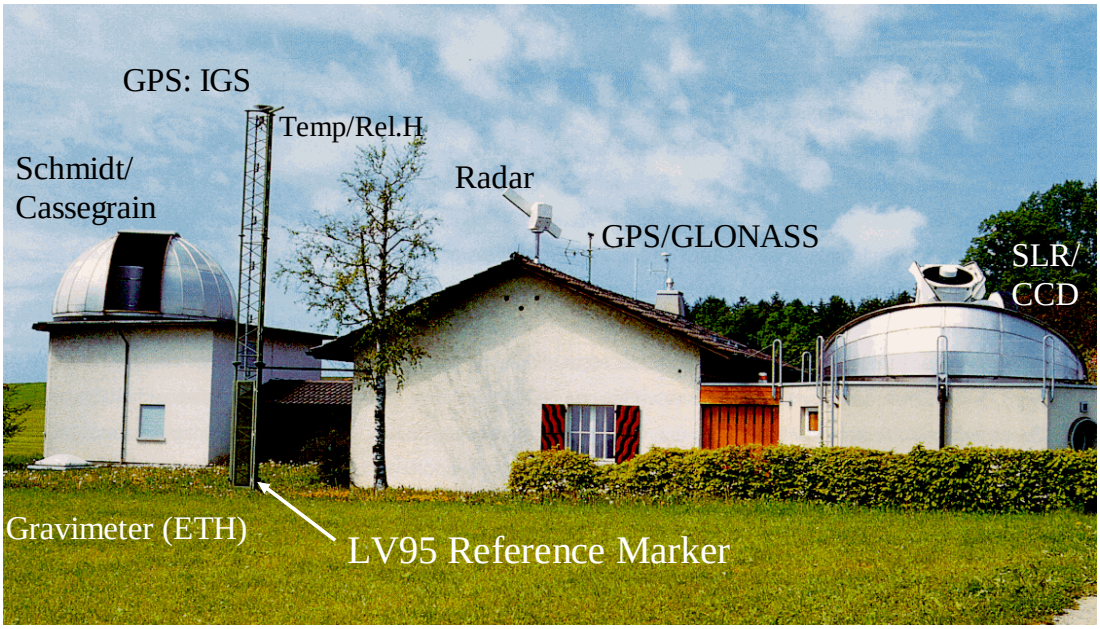

Figure 1: *The Zimmerwald Observatory*

The Zimmerwald Laser and Astrometric Telescope ZIMLAT

The main characteristics of the telescope are as follows:

The diameter of the main mirror is one meter. The telescope is of the Ritchey-Chretien type with main mirror, secondary mirror and a flat 45-degree tertiary mirror reflecting the image sideways into the elevation axis.

A vertical platform on one side of the telescope serves as mounting surface for four optical tables, with reduction optics, filter wheels and CCD cameras (Figure 2). The platform can be rotated around its horizontal axis (independent from the motion of the tube around the elevation axis) to derotate the image on the camera according to various strategies. The camera to be used for observation can be selected by means of a rotating mirror (with four distinct positions) in the center of the platform.

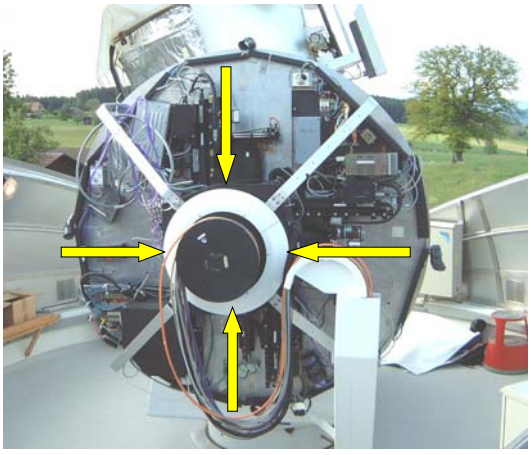

Figure 2: *Instrument platform*

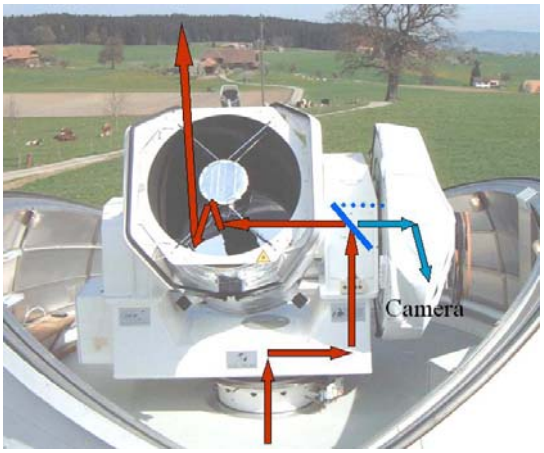

Figure 3: *ZIMLAT telescope*

For Satellite Laser Ranging the laser beam is guided, slightly off-axis, through the Coudé path to the telescope (Figure 3). Its diameter of 1 cm at the exit of the transmit table is increased to 15 cm by the telescope optics. The receiving beam fills the full aperture of the telescope as well as the Coudé path back to the receiving table.

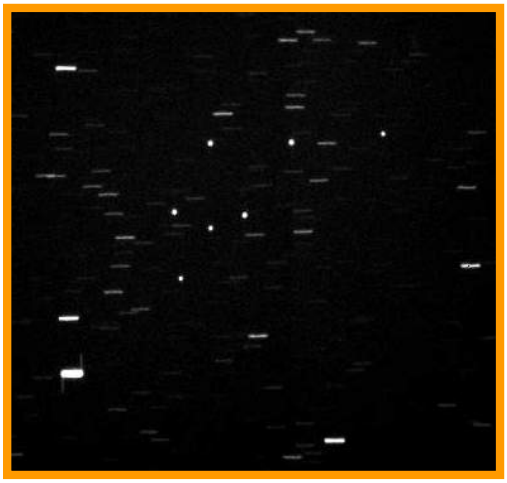

Figure 4: *7 Geostationary Astra satellites (field of view 12x12‘)*

Figure 4 shows a sample image of one of the CCD cameras with 7 geostationary satellites within a field of view of about 12 arc minutes squared. The telescope was

kept fixed during the exposure time, showing the daily rotation of the Earth as short traces of the background stars.

The separation between the CCD and SLR observation modes is done by a fairly large dichroic 45-degree beam splitter mirror in the elevation axis of the telescope. It can be pneumatically removed (tilted) for high-precision CCD imaging. During night-time SLR tracking a video camera on one of the four camera ports can be used for visual verification of the tracking with the dichroic beam splitter inserted.

The Control Systems

The Satellite Laser Ranging part is controlled by the program *ZIMLAS* running on an Alpha workstation (operating system: VMS). It communicates with two specialized PCs for data collection and control of various electronic components and for the control of the telescope. The workstation handles the satellite predictions, generates the observation schedule (example in Figure 6), stores and post-processes the range observations, interacts with the operator in manual mode or controls the whole system in fully automated mode (see also Gurtner et al, 2002).

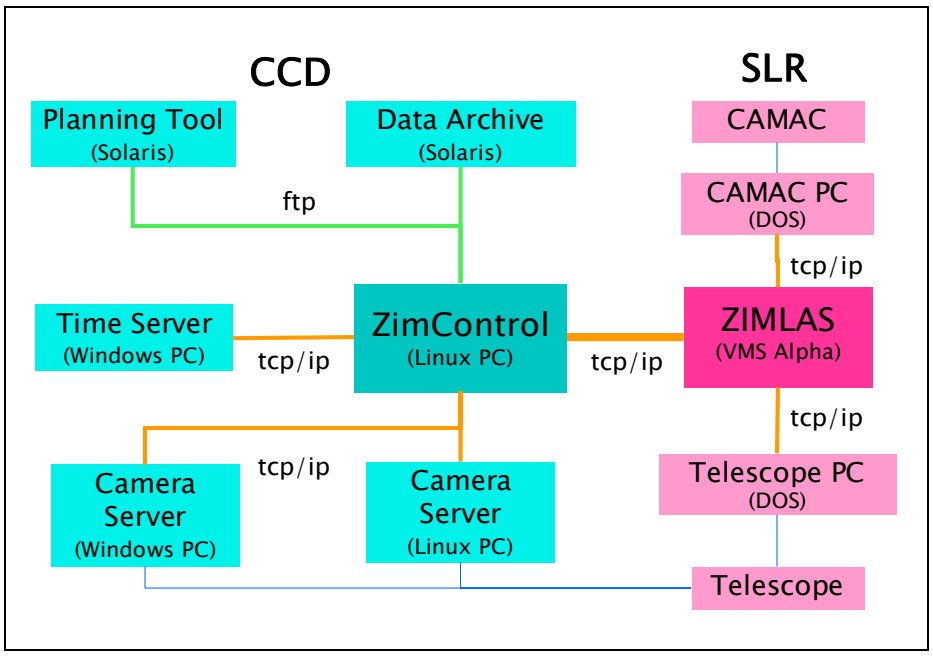

Figure 5: *Control Systems*

The control system for CCD observations (program *ZimControl*) is hosted by a Linux PC. It handles the observation schedule for CCD observations, interacts with the CCD cameras through specialized camera servers, and stores and pre-processes the digital images.

CCD Targets and Observation Plan

The following targets and objects are routinely tracked

- GEO (geostationary objects)
  - Active satellites
  - Space debris
- GTO (geostationary transfer orbit): Upper stages, debris
- Minor planets: Confirmation exposures for Near-Earth Objects

- GPS satellites to check system status (e.g., timing system)
- Photometry: Change of visual magnitude of objects due to their rotation
- Bias and dark current exposures (camera properties)
- Projection parameters, image distortions (telescope and camera properties)
- Focussing exposures (temperature- and elevation-dependent)

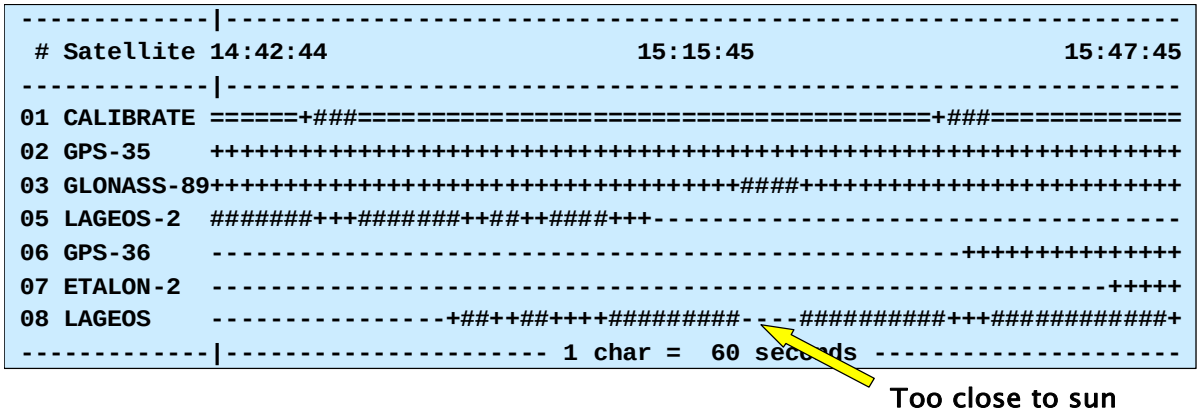

Figure 6: *Automatically generated observation schedule (SLR)*

Figure 7 shows an observation plan with targets and their possible observations periods during one night.

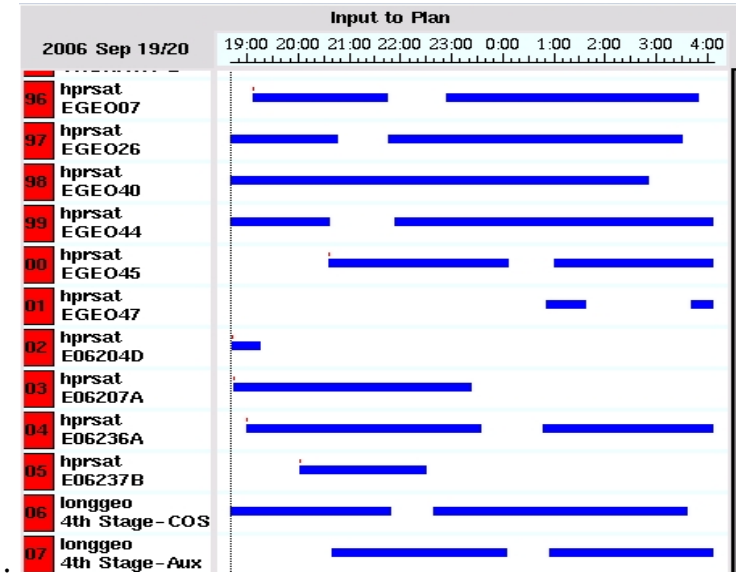

Figure 7: *CCD observation plan*

Insertion of CCD observations into SLR operations

Whenever the sun is more than 9 degrees below the horizon the CCD control system automatically checks if the SLR tracking system is currently operating.

If it is and if there are suitable objects in the observation plan the CCD system starts requesting observation time from the SLR system, starting with a time slot of 10 minutes, gradually reducing its length down to a minimum of 3 minutes if the request is not granted. This process is repeated over and over until a request is granted.

On the other side the SLR system checks each request, compares the requested duration with the current SLR tracking scheme and grants or rejects the request

according to the following conditions:

- Time since last CCD observation “large enough”
- Remaining pass segment of current SLR target “large enough”
- Already a minimum number of successful SLR observations collected
- Currently not in calibration mode
- CCD mode not blocked by operator

“Large enough” depends on the priority of the current SLR target and on the priority assigned to CCD operations.

If the request is granted the SLR system interrupts the current SLR tracking, puts the telescope into CCD mode (removal of the dichroic beam splitter from the elevation axis, pointing of the selection mirror on the platform to the requested CCD camera) and sends the requested object position or trajectory to the telescope control PC for tracking.

The CCD control system commands the camera to take an exposure and stores the digital image for further processing. Depending on the length of the granted observation interval several images of the same object or of different objects may be collected.

At the end of the current CCD observation interval the SLR system puts the telescope back into SLR mode and continues to range to the SLR targets according to the automatically updated tracking scenario.

The CCD control system then starts all over again with new requests for CCD tracking as long as the SLR system is in operation and until dawn.

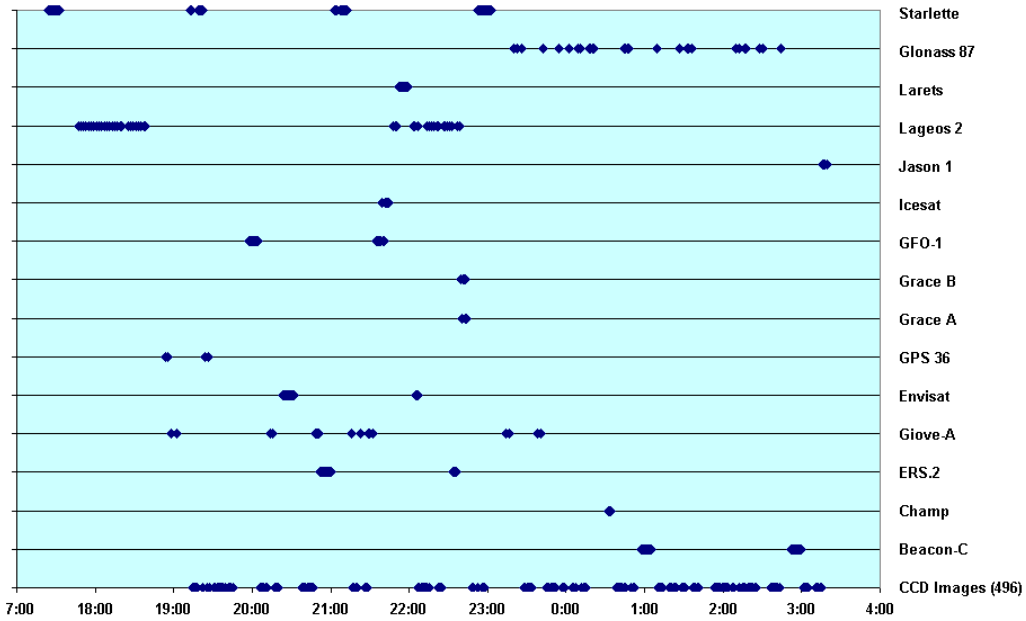

***Figure 8**: SLR/CCD interleaving*

Switching between the two modes SLR and CCD needs all in all less than 30 seconds, repositioning of the telescope included. Figure 8 shows the actual tracking scenario (SLR satellites, CCD observations on the bottom line) of the night of September 1st, 2006. Thanks to the rapid interleaving of CCD into SLR, especially into the long passes of medium-high (Lageos 1,2) and high satellites (navigation satellites and Etalon 1,2) no substantial reduction of the SLR data output could be observed.

Figure 9 shows the monthly number of images collected during the last one and a half years.

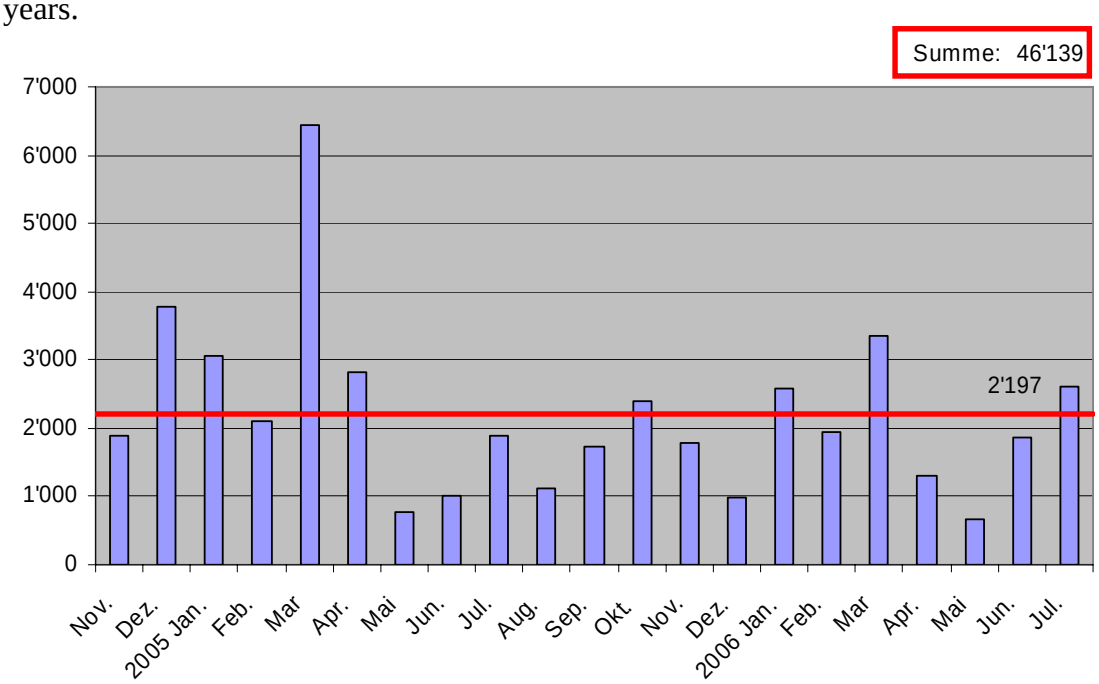

Figure 9: *Monthly number of CCD images Nov 2004 - Jul 2006*

Automation

The two control programs SLR and CCD are independent programs (running on two different computer systems). Either one or both can run completely automatically and unattended or under operator control.

In the extreme case (good and predictable weather conditions provided) several observation sessions of a few hours length each can be set up and submitted in advance by simple commands like

```
AUTO_SLR 20:00 22:00 WG MEDIUM
```

defining start and end time of the session, responsible observer's initials, and the priority assigned to CCD observations. All the rest is taken care of by the two control systems.

Post-processing

SLR data post-processing, i.e.,

- computation and application of an average calibration constant
- data screening
- normal point generation
- exchange format generation and submission of the data to the ILRS data center

can either be done interactively (daylight: mandatory) or fully automatically.

Image processing is automated and runs in the background on a Linux system at the university (the image files are automatically transferred to the university right after acquisition):

- Object recognition
- Reference star selection
- Determine image positions of stars and objects

- Astrometric position of objects
- Image archiving

The automatic processing of the previous night is checked interactively and problematic cases are reprocessed manually.

Conclusions

The dual use of the Zimmerwald Laser and Astrometric Telescope ZIMLAT has proven to be very cost-efficient. Although the telescope's design and operation is more complicated than the one of a single-mode instrument it provides us two different observation techniques for little more than the costs of a simple telescope. Thanks to the high degree of automation the two modes can be used nearly simultaneously without significant reduction of the SLR data output.

References

[1] Gurtner W., E. Pop, J. Utzinger (2002), *Improvements in the Automation of the Zimmerwald SLR Station*, 13th International Workshop on Laser Ranging, October 7-11, 2002, Washington, D.C.

Automated Transmitter Beam Size and Divergence Control in the SLR2000 System

J. Degnan, G. Jodor, and H. Bourges

1. Sigma Space Corporation, 4801 Forbes Blvd., Lanham, MD 20706 USA.

Contact: John.Degnan@sigmaspace.com /Fax: +01-301-577-9466

Abstract

Signal count rates and orbital time bias estimates vary widely over the range of satellite altitudes. In order to obtain an acceptable photon count rate for the higher satellites (e.g. LAGEOS, ETALON, GPS) while still meeting eye safety requirements at the telescope exit aperture, we must tightly control both the SLR2000 transmit beam diameter at the exit aperture and the final beam divergence half angle. For lower satellites, the uncertainty in the satellite angular position and the signal count rates are both relatively high. Thus, the SLR2000 design targets a nominal range of beam divergence half angles between 4 arcsec (larger than the combined effects of mount pointing jitter and atmospherically induced spreading and beam wander) for high satellites and 13 arcsec (adequate to accommodate time bias uncertainties) for LEO satellites. A modified commercial beam expander in the transmitter is used to maintain a constant transmitter beam size at the telescope exit aperture for eye safety while simultaneously varying the beam divergence to accommodate the various satellite altitudes and angular uncertainties.

Introduction

SLR2000 adjusts transmitter beam divergence based on satellite altitude and orbital knowledge, i.e. narrower for high satellites (± 4 arcsec min) and wider for low satellites (± 13 arcsec max). For eye safety reasons, the divergence must be adjusted while keeping the beam diameter at the telescope exit aperture fixed. It has been shown [Klein and Degnan, 1972] that a ratio of telescope diameter to Gaussian beam diameter (between $1/e^2$ intensity points) equal to 1.12 maximizes the amount of energy on the satellite. Thus, for the 40 cm SLR2000 telescope, the optimum beam diameter is 35.7 cm, and final divergence is set by adjusting the phase front curvature of the transmit beam at the telescope exit window. The Special Optics Beam Expander (SOBE) for controlling spot size and divergence is located on the transceiver bench in the transmitter path. This paper outlines our technical approach and additional details can be found elsewhere [Degnan, 2005].

Paraxial ray matrix theory can be applied to Gaussian laser beams if the beam is represented by the complex parameter

$$\frac{1}{q(z)} = \frac{1}{R(z)} - j\frac{\lambda}{\pi\omega^2(z)} \qquad (1)$$

where λ = 532 nm is the laser wavelength in the propagation medium and R(z) and ω(z) are respectively the wavefront curvature and spot radius (measured from the beam center to the $1/e^2$ intensity point) of the Gaussian beam at the location z along the propagation axis. If $q(z_0)$ is the Gaussian beam parameter at the output of the SOBE, then the Gaussian beam parameter at the exit window of the telescope is given by the ABCD Law [Verdeyen, 1989]

$$\frac{1}{q(z)} = \frac{C + D\left(\frac{1}{q(z_0)}\right)}{A + B\left(\frac{1}{q(z_0)}\right)} \tag{2}$$

In (2), A, B, C, and D are the ray matrix coefficients which propagate the rays from the SOBE to the telescope exit aperture. Separating (2) into its real and imaginary parts yields the following expressions for the wavefront curvature and beam spot size at the telescope exit aperture, i.e.

$$R(z) = \frac{\left(A + \frac{B}{R(z_0)}\right)^2 + \left(\frac{B\lambda}{\pi\omega^2(z_0)}\right)^2}{\left(C + \frac{D}{R(z_0)}\right)\left(A + \frac{B}{R(z_0)}\right) + BD\left(\frac{\lambda}{\pi\omega^2(z_0)}\right)^2} \tag{3a}$$

and

$$\omega(z) = \omega(z_0)\sqrt{\left(A + \frac{B}{R(z_0)}\right)^2 + \left(\frac{B\lambda}{\pi\omega^2(z_0)}\right)^2} \tag{3b}$$

We can now compute the ABCD matrix for the transmitter at the satellite target by multiplying the system matrix by the propagation matrix and letting the target range, *r*, approach infinity, i.e.

$$FF = \lim_{r\to\infty}\begin{vmatrix} I & rI \\ 0 & I \end{vmatrix}\begin{vmatrix} A\Gamma' & B\Gamma' \\ C\Gamma' & D\Gamma' \end{vmatrix} = \lim_{r\to\infty}\begin{vmatrix} (A+rC)\Gamma' & (B+rD)\Gamma' \\ C\Gamma' & D\Gamma' \end{vmatrix} \cong \begin{vmatrix} rC\Gamma' & rD\Gamma' \\ C\Gamma' & D\Gamma' \end{vmatrix} \tag{4}$$

Substituting A = rC and B = rD into (3) yields the following expressions for the phase front curvature and spot size at the satellite

$$R(r) = r \tag{5a}$$

and

$$\omega(r) = r\omega(z_0)\sqrt{\left(C + \frac{D}{R(z_0)}\right)^2 + \left(\frac{D\lambda}{\pi\omega^2(z_0)}\right)^2} = r\frac{\omega(z_0)}{m_t}\sqrt{\frac{1}{R^2(z_0)} + \left(\frac{\lambda}{\pi\omega^2(z_0)}\right)^2} \tag{5b}$$

where, for SLR2000, C = 0 and D = $1/m_t$ = 0 where m_t = 30.48 is the total magnification in the transmit path [Degnan, 2005]. As expected, the wavefront curvature in the far field equals the distance from the telescope aperture and the spot size grows linearly with that distance. Equation (5b) can therefore be used to compute the beam divergence half angle (center to $1/e^2$ intensity point) of the transmitter in the far field, i. e.

$$\theta_t \equiv \frac{\omega(r)}{r} = \frac{\omega(z_0)}{m_t}\sqrt{\frac{1}{R^2(z_0)} + \left(\frac{\lambda}{\pi\omega^2(z_0)}\right)^2} = \frac{\lambda}{\pi m_t \omega(z_0)}\sqrt{1 + \left(\frac{\pi\omega^2(z_0)}{\lambda R(z_0)}\right)^2} \tag{6}$$

Note that the far field divergence depends on both the spot size, $\omega(z_0)$, and the phase front curvature, $R(z_0)$, at the output of the SOBE.

Technical Approach

The approach we followed for controlling SLR2000 beam size and divergence was as follows:

1. Measure transmitter gaussian beam radius (.969 mm) at entrance plane to beam expander, raw beam half divergence, and compute gaussian complex q-parameter for the input beam
2. Choose a COTS beam expander with an adequate exit aperture (>40cm/30.48 = 13.1 mm) and magnification range (~13.1 mm/ 2mm = 6.5) and at least two control elements for independently adjusting beam size and phasefront curvature at the output.
3. Develop dynamic ray model for unit including variable lens spacings.
4. Test dynamic ray model against sophisticated ray tracing program such as ZEMAX.
5. Calibrate beam expander servo controllers at various magnifications.
6. For each divergence value, use the gaussian beam propagation law to compute the complex q-parameter of the expander output beam and the lens spacings which produce that parameter.
7. Compute lookup table specific to laser transmitter

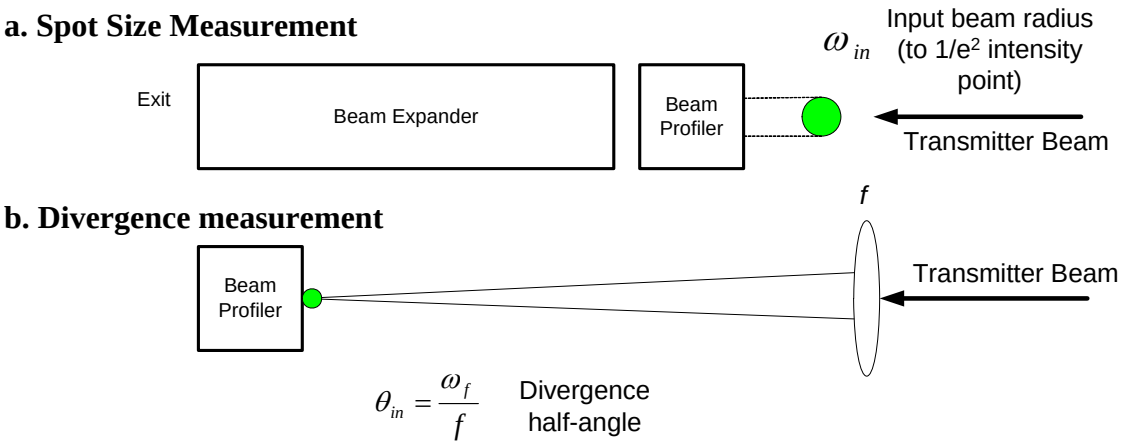

***Figure 1**: Measuring the Gaussian parameters of the raw transmit beam: (a) input radius; and (b) far field beam divergence.*

The beam radius and divergence of the transmitter beam at the input to the SOBE were measured using a standard beam profiler as in Figure 1. The complex Gaussian beam parameter was then computed from the formula

$$\frac{1}{q_{in}} \equiv \frac{1}{R_{in}} - j\frac{\lambda}{\pi\omega_{in}^2} = \frac{\lambda}{\pi\omega_{in}^2}\left(\sqrt{\left(\frac{\pi\omega_{in}\omega_f}{\lambda f}\right)^2 - 1} - j\right) \tag{7}$$

The commercial version of the Special Optics Beam Expander Model 56C-30-2-8X is normally operated under a Labview environment and is designed to provide a wide range of beam magnifications (2X to 8X) at the desired wavelength. Sigma has reconfigured the unit to operate with two National Aperture Motor Controllers under a more flexible software control. The optical unit consists of five lenses: a moving singlet at the input end, a moving doublet in the middle, and a larger aperture stationary doublet at the output end as in Figure 2. The moving singlet and doublet are

driven by two independent stepper motors. Their positions are determined by counting the number of steps from a home position as defined by two limit switches.

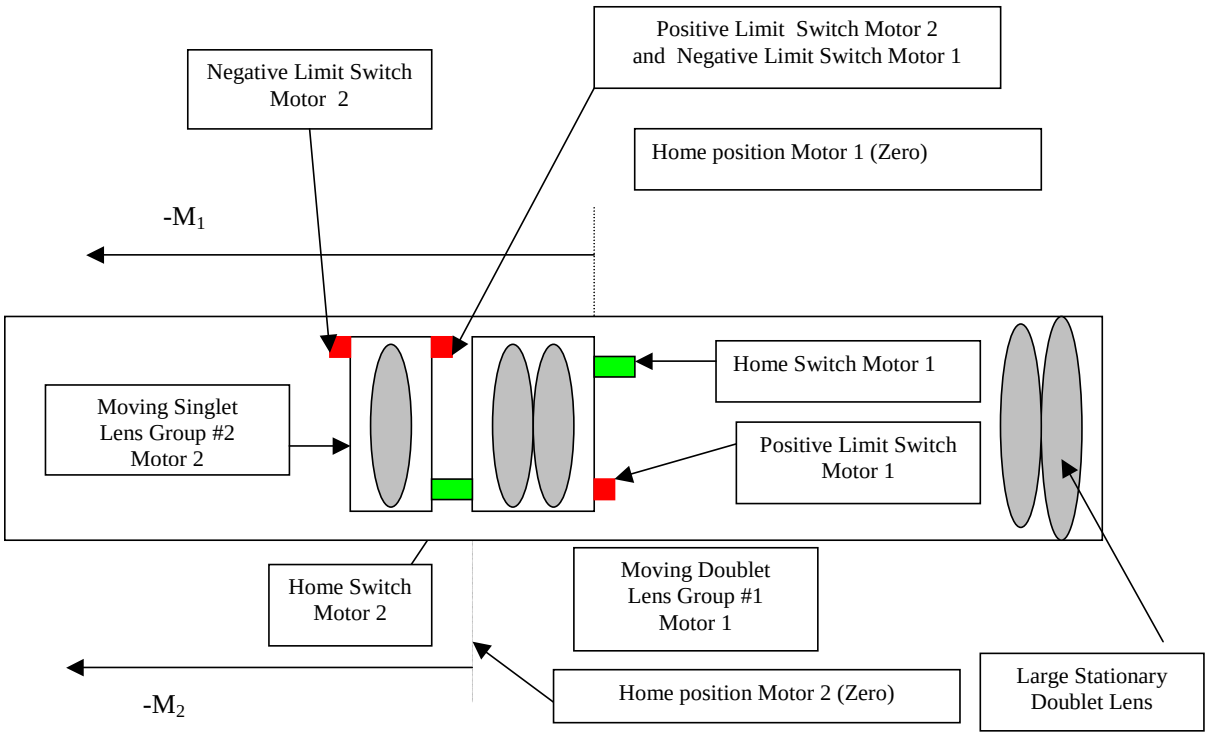

Figure 2: *Optomechanical configuration of Special Optics Beam Expander Model 56C-30-2-8X. The expander has entrance and exit apertures of 10 mm and 30 mm respectively.*

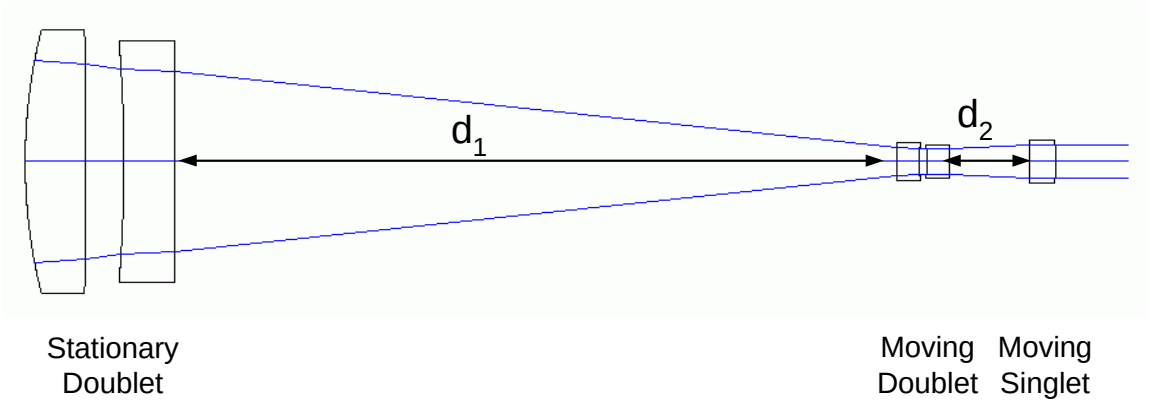

Figure 3: *Optical layout of Special Optics Model 56C-30-2-8X Beam Expander.*

Using an optical prescription provided by Special Optics, we computed a "dynamic ray matrix" for the SOBE depending on the variables d_1 and d_2 defined in Figure 3. The result was

$$M_{SO}(d_1,d_2)=\begin{vmatrix} A_{SO}(d_1,d_2) & B_{SO}(d_1,d_2) \\ C_{SO}(d_1,d_2) & D_{SO}(d_1,d_2) \end{vmatrix} \tag{8}$$

where

$$A_{SO}(d_1, d_2) = A_0 + A_1 d_1 + A_2 d_2 + A_{12} d_1 d_2 \tag{9a}$$

$$B_{SO}(d_1, d_2) = B_0 + B_1 d_1 + B_2 d_2 + B_{12} d_1 d_2 \tag{9b}$$

$$C_{SO}(d_1, d_2) = C_0 + C_1 d_1 + C_2 d_2 + C_{12} d_1 d_2 \tag{9c}$$

$$D_{SO}(d_1, d_2) = D_0 + D_1 d_1 + D_2 d_2 + D_{12} d_1 d_2 \tag{9d}$$

and the computed coefficients appearing in (9) are summarized in Table 1.

Table 1: *Summary of coefficients appearing in the SOBE ray matrix*

Suffix	A	B	C	D
0	1.995665379968	0.028752151456	46.402866180544	1.170293617808
1	63.683551232	1.442710470656	-460.710690944	-10.437108561152
2	-45.765735168	2.505955512	-1230.503704704	67.377646836
12	-1634.569158656	89.502715904	11825.086257152	-647.496210368

Setting C_{SO} =0 and A_{SO} equal to integer magnifications between 2 and 8, the ray matrix predictions of the interlens spacings, d_1 and d_2, computed from (9a) and (9c) were then compared to those of a popular ray tracing program, ZEMAX, and the predictions were found to agree within a few tens of microns for all magnifications. The two motor positions, relative to their respective home limit switches, are related to the interlens spacings via the equations

$$M_1 = a - d_1 \quad \text{and} \quad M_2 = b - d_1 - d_2 \tag{10}$$

Following our inhouse calibration procedure, the constants a = 88.7412 mm and b = 92.9858 mm in (10) were found to differ from the values (a = 88 mm and b = 90 mm) provided by the manufacturer. The next step in the process is to tabulate the values of d_1 and d_2 that produce the desired spot size and divergence at the exit aperture of the telescope. This is accomplished by using the Gaussian propagation law (2) to generate the following approximate expressions for the beam radius and phasefront curvature at the exit aperture of the SOBE

$$\omega_0(\theta_t) \cong \frac{\omega}{m_t} - d_t\theta_t = 0.00585 - 30.84\theta_t(rad)$$

$$\frac{1}{R_0(\theta_t)} \cong \frac{m_t^2\theta_t}{\omega - m_t d_t \theta_t} = \frac{929.0\theta_t\,(rad)}{0.1785 - 940.0\theta_t(rad)}\, m^{-1}$$

where ω = 0.179 m and θ_t, are the desired beam radius and beam divergence at the telescope exit aperture. For each divergence, we then use the beam expander ray matrix (8) to compute the expander lens positions, $d1$ and $d2$, which yield the above values of ω_0 and R_0. The final step is to compute the corresponding motor positions via (10), convert the latter into encoder counts using a scale factor of 0.304 microns per step, and generate a table lookup of beam divergence versus encoder counts for each motor. Figure 4 gives a graphical representation of the interlens separations in the lookup table as a function of final transmitter beam divergence for SLR2000.

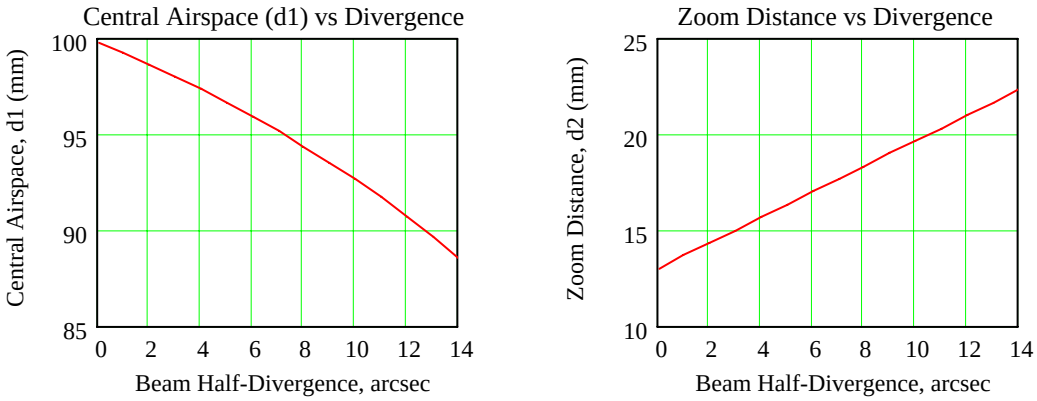

Figure 4: *The computed interlens distances, d_1 and d_2, in the SOBE which produce a given divergence half-angle in the far field while maintaining a constant spot radius of 17.9 cm at the exit aperture of the telescope. A circularized Phase II laser with a mean Gaussian radius of 0.969 mm and a raw half-divergence of 1.265 mrad is assumed as input to the SOBE.*

Summary

Using a computer lookup table, the SLR2000 computer can set two lens spacings in the 5-element transmit beam expander to provide a fixed beam diameter (35.8 cm) at the telescope exit aperture for eye safety while adjusting the phasefront curvature to give the desired final divergence. The lookup table must be updated whenever the transmitter is changed but it is an automated process. The optical half-divergence range of the final SLR2000 transmit beam is theoretically 0.25 arcseconds to 13 arcseconds (1.3 to 65 microradians) but atmospheric turbulence will define the actual lower limit. For verification, GSFC monitors the divergence of the SOBE output via a long focal length lens and CCD camera as outlined in Figure 1 and divides the result by the total magnification in the transmitter path. Presently, an inadvertent defocus in the SLR2000 main telescope is being compensated for by an offsetting defocus in a 3-power telescope on the transceiver bench. As a result, the nominal magnification of 30.48 for perfectly focused telescopes has been reduced to 28.21 for the compensated telescopes [Degnan, 2005].

References

[1] Degnan, J. J., "Ray Matrix Analysis for the Realtime Control of Automated SLR2000 Optical Subsystems", Chapter 8, Sigma Space Corporation Report, October 2005.

[2] Klein, B. J. and J. J. Degnan "Optical Antenna Gain. I. Transmitting Antennas", Applied Optics, 13, pp. 2134-2141, 1974.

[3] Verdeyen, Joseph T., Laser Electronics, Chapter 5, Prentice Hall, Englewood Cliffs, New Jersey 1989.

Obtaining the High-resolution Epoch with the FPGA Technology

Q. Li, F. Qu and Z. Wei

1. Chinese Academy of Surveying and Mapping (CASM)

Contact: liqian@casm.ac.cn /Fax:0086-10-68218654

Abstract

In Satellite Laser Ranging it is important to record the transmission epoch of each laser pulse. Currently in the Beijing SLR station many counter-chips are used to accomplish this task. With the popularity of the FPGA technology, engineers find that using FPGA (Field Programmable Gate Array) to design the digital system is a feasible way to reduce the dimension of the circuit board and increase the reliability of the system. We are designing a new epoch measurement system using one Xilinx's Spartan FPGA chip to accomplish what previously had required many counter-chips. The 1pps signals and the time code from the HP58503 are used to get rough epoch information to a one second resolution. The 10 MHz frequency from the HP58503 is used as the system clock. A 24-bit counter module in the FPGA chip, used with the system clock, gives timing information with a resolution of 100 nanoseconds and with a period of one second. To obtain the time code from the HP58503, two UART (Universal Asynchronous Receiver) modules are used, one to communicate with the HP58503, and another to transfer the epoch data to a PC.

Introduction

Fig.1 shows the present module at the Beijing Station that is used to obtain the epoch of the laser pulse. It is the cascade connection of 6 counter-chips. Every chip is only 4 bits, so higher resolution requires more counter-chips. To achieve a higher integrated level, we selected the FPGA chip which would perform the same task in a single module.

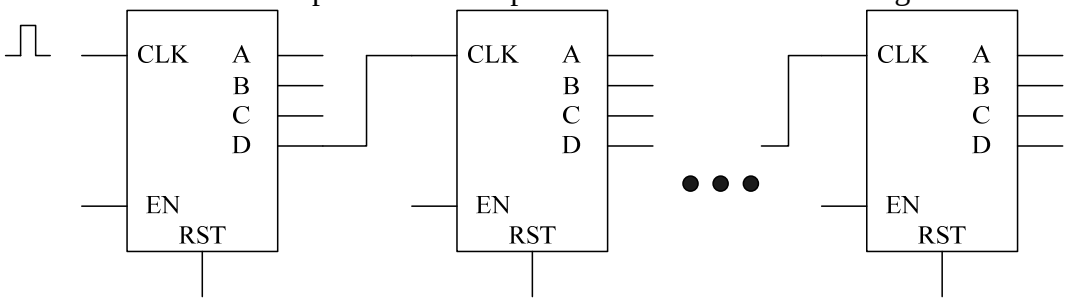

Figure 1: *Present module to obtain the epoch in Beijing Station*

Fig.2 shows the block scheme of the system. The HP58503 supplies the reference frequency, the one-pulse-per-second signal and the time code for the FPGA module to establish a UTC time clock. When a laser pulse arrives, the FPGA module sends the epoch data to the PC through the Serial Interface. MAX3232 is used as the level translator between the RS232 and LVTTL.

Establishment of the UTC time clock

Fig.3 shows the block scheme of the establishment of the UTC time clock. As the input clock frequency is 10MHz, so the time resolution is 100ns. To record one complete second, we must use a counter with at least 24 bits, because,

$$\log_2 \frac{1}{100 \times 10^{-9}} = 23.3$$

It’s convenient to design a 24-bit counter in FPGA. Another 16-bit counter is designed to record the number of 1pps events after the reset operation. The 16-bit counter can record the time up to 18 hours, so 18 hours later, another reset operation is needed. Some registers are used to record the time code from the HP58503 to save the datum time.

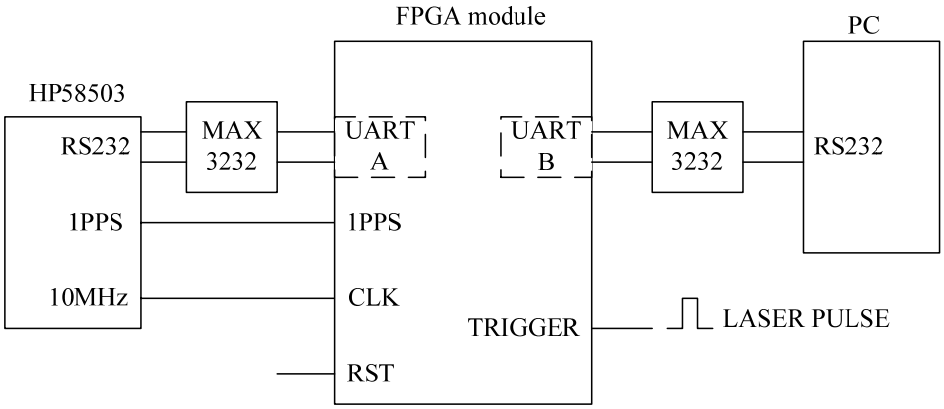

Figure 2: *Block scheme of the system*

Obtaining the epoch of the laser pulse

When a laser pulse arrives, some relative-time-registers are allocated to store the current values of REG1 and REG2. Then the data in the datum-time-registers and relative-time-registers are sent to the PC through UART B. The PC performs the final calculations required to obtain the transmission epoch of the laser pulse.

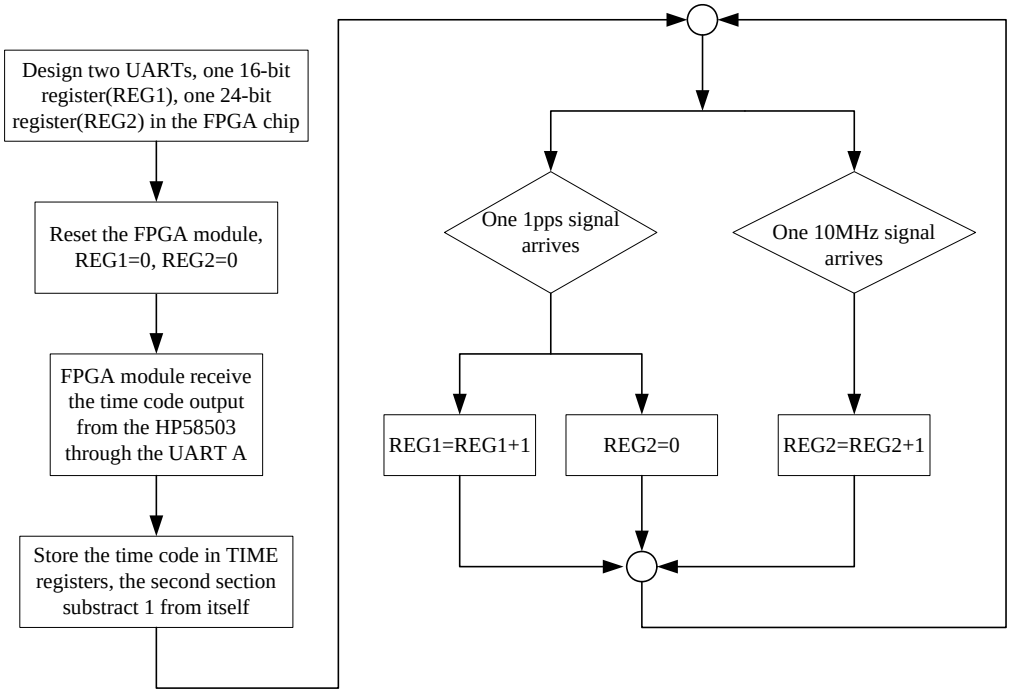

Figure 3*: The Establishment of the UTC time clock*

Comparison experiment and conclusion

A test setup has been designed to make sure that the new module can obtain the time code, 10MHz signal, 1pps signal from HP58503 as well as the laser pulse without disturbing the original system. Comparing the two epoch data shows that the new module has the equivalent function to the original one.

Difficulties in the development process and Future Plans

In the development process, the implementation of the UART is relatively harder than that of the counters. So compared with the microprocessors, the merits and drawbacks of developing a digital system with an FPGA are obvious.

Today, RISC microprocessors with an ARM core are widely used to design digital systems, so the structure “ARM+FPGA” may be a good choice for developing a digital system that can achieve higher resolution, precision, stability, flexibility and integration level as well as shorten the development time.

Platform

- Device:

  - Xilinx’s Spartan FPGA, HP58503, PC

- Software:

  - Xilinx ISE 7.1

  - VC++ 6.0

- Top-level Module type

  - HDL(Verilog HDL)

- Simulator

  - ISE Simulator

- Synthesis

  - XST(VHDL/verilog)

NEW FTLRS software tools for tuning observations schedule and remote control

Monique Pierron and FTLRS staff

1. Observatoire de la Côte d'Azur, Avenue N.Copernic - 06130 Grasse – France.

Contact: Monique.pierron@obs-azur.fr

Abstract

In the goal to facilitate and make more pertinent campaign observations, we have developed:

- *A fully automated mechanism for the CPF predictions: CPF file reception and propagation, prediction generation and orbit display are automatically performed.*
- *An acquired data sky coverage display for any site (per satellite and per date).*
- *A new levelling system for FTLRS, easy to use for observers, efficient and completing the remote controlled capability.*

Introduction

The French Transportable Laser Ranging Station often operates far from our French location in Grasse and it is very important to increase its remote capability, and to facilitate the observer's life.

Fully automated mechanism for the predictions

CPF mail reception

Mail is automatically extracted on the principal computer in Grasse. CPF files are sorted and dispatched in dedicated directories (for example /d/dat/prev/grca if GraceA) and files. File names are based on CPF file headers, for example gracea_060930_7732.gfz is done with target (gracea), date (060930), sequence number (7732) and provider (gfz).

CPF file propagation for FTLRS

For this, we use the rsync command (a free software computer program for Unix) to synchronize CPF files and directories from the Grasse computer to the FTLRS computer. This rsync command is executed every hour via the Crontab unix facility.

Files creation for satellite orbit display

All necessary files to display satellite orbits for the next few hours are created daily on Grasse and FTLRS computers (via cron facility):

- satellite timetable files for one month or more,

- prediction files for satellite passes to come: in this file, the step between positions depends on pass duration, in order to have a continuous curve for orbit display,
- file with next passes list for easy display; each line has the following form: Satellite name, MJD (begin), culmination, azimuth (begin and end), duration, date (hour and minute), prediction file name.

Satellite list and orbit display

At login the following window is displayed and continuously updated.

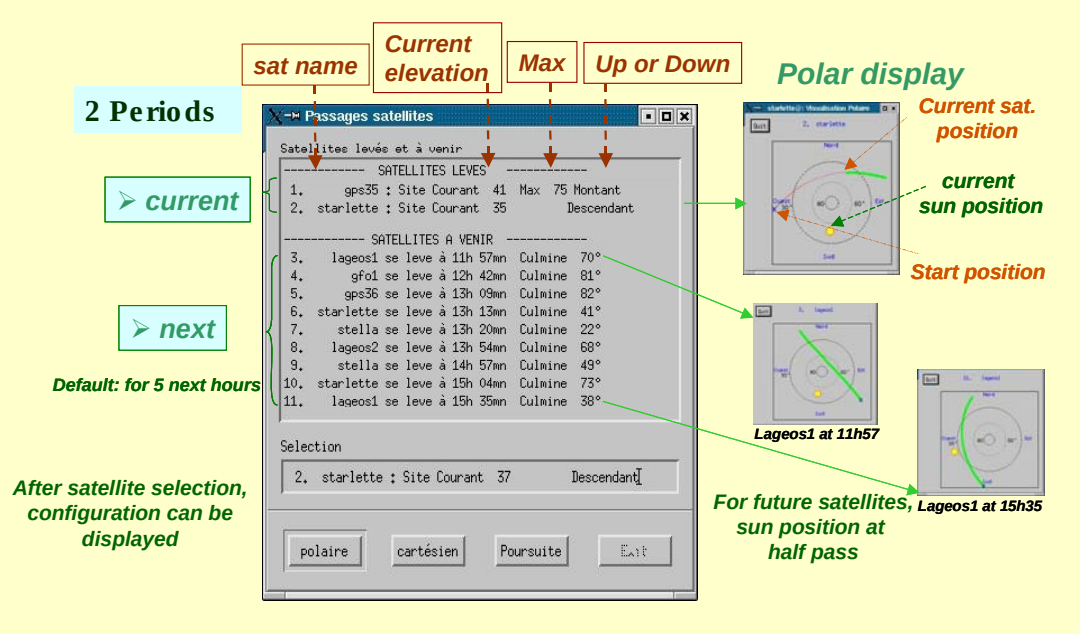

A few minutes before each satellite pass, a window with information appears and a bell rings.

With this mechanism in place, it was then natural and easy to develop the prediction's server on our main computer in Grasse. An executable prediction client (for Windows and Linux) is available. This will be very useful for further operations with MEO station (7845).

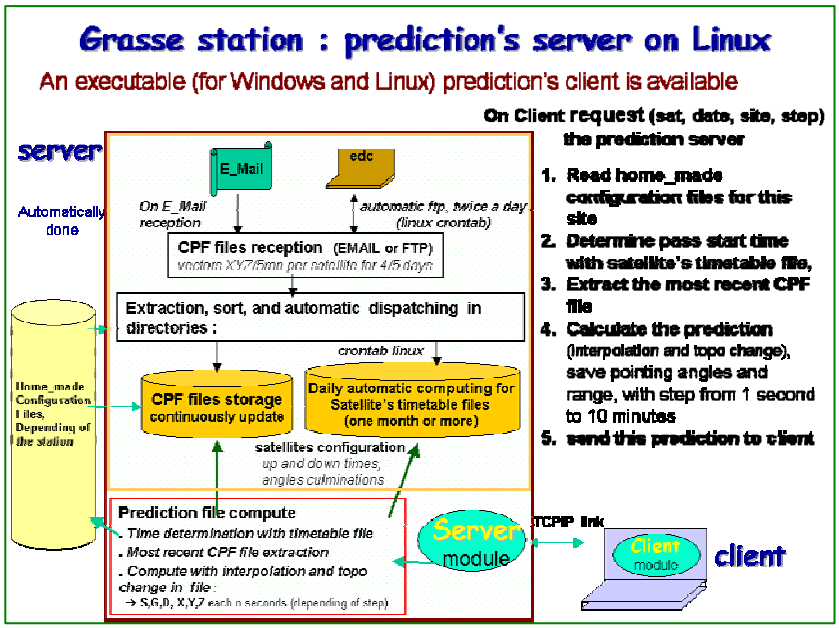

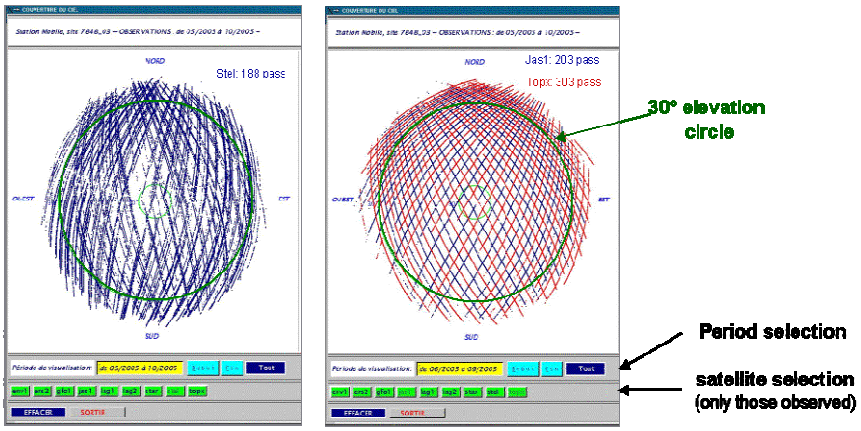

***Figure 1**: Sky coverage for Stella and Jason/Topex - FTLRS - May to October 2005*

Acquired data sky coverage display

This application allows display of data for each Grasse station (FTLRS, MEO and GRSL). Each point on the display is a validated return. The operator has just to choose:

- the satellite(s) in the proposed list, and
- the observation period.

The observation's Grasse station is done with an environment's variable.

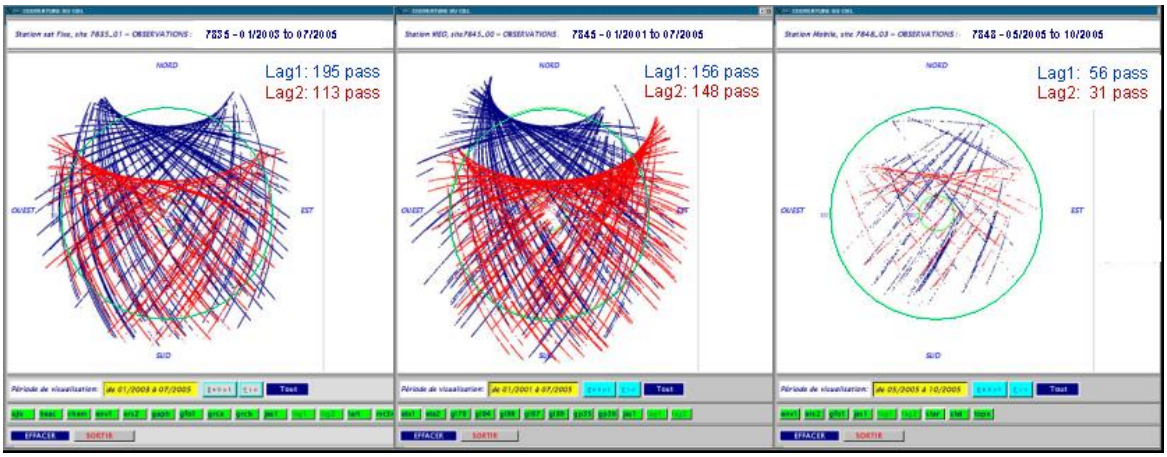

***Figure 2**: Lageos 1/Lageos 2 on Grasse stations: GRSL(7835), LLR(7845) and FTLRS (7848 Ajaccio)*

For FTLRS (7848 station during last Corsica campaign), we observe from the display that:

- the coverage has good repartition on all directions,
- Stella (first part Figure 1) is lost just during culmination,
- for Lageos (third part Figure 2) there were no returns under 30 or 40 degrees.

For GLRS (7835 station) we had a good coverage for all satellites (low satellites to Lageos).

For 7845 station (MEO station used for HEOS) from Lageos:

- the coverage has good repartition on all directions,
- it is easy to have returns when the satellite is low,
- for Lageos, it is very difficult to have returns when higher than 80°; this doesn't exist for higher satellites (Glonass or GPS).

A remote levelling system for FTLRS

We have developed a new system, to process the mount levelling system. The system (laser + telescope) is now on a mechanical device, and this device is levelled with two electrical jacks. These jacks are positioned in perpendicular directions.

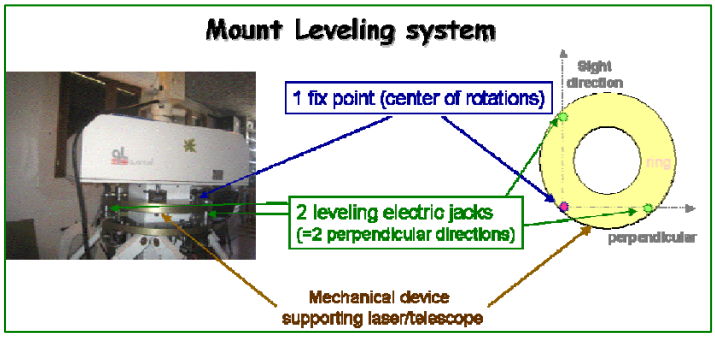

Figure 3: *The new mount Levelling sytem for FTLRS*

These jacks are software controlled via a control panel. Levelling values in two directions are continuously read and displayed, and it is possible to adjust the level:

- manually with the two push buttons on panel, or
- automatically with a servo loop control.

This new remote tool for FTLRS is efficient, easy to use and very important for remote controlled capability.

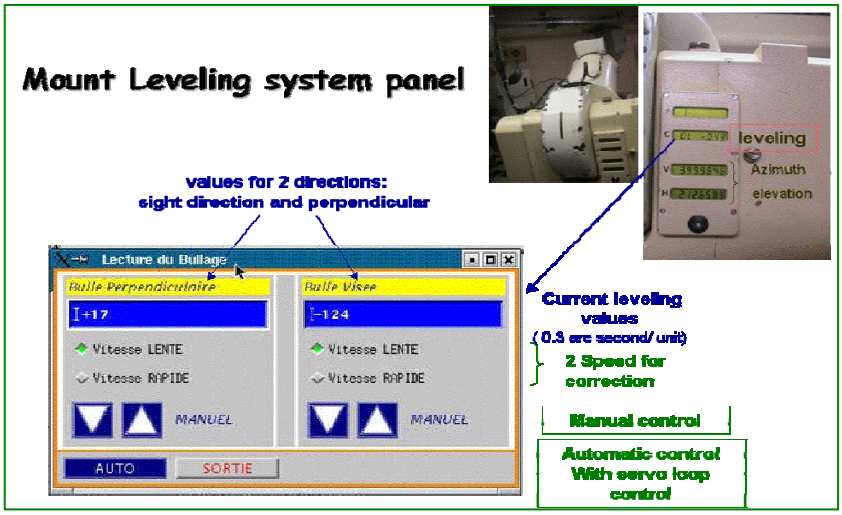

Conclusion

Fully automated mechanisms for the predictions and the new levelling system for FTLRS are major improvements, facilitating the observer's life and completing the remote controlled capability. FTLRS will very soon be operational in our new laboratory in Grasse, and all our staff is very excited to test these new tools and we look forward to our first returns there.

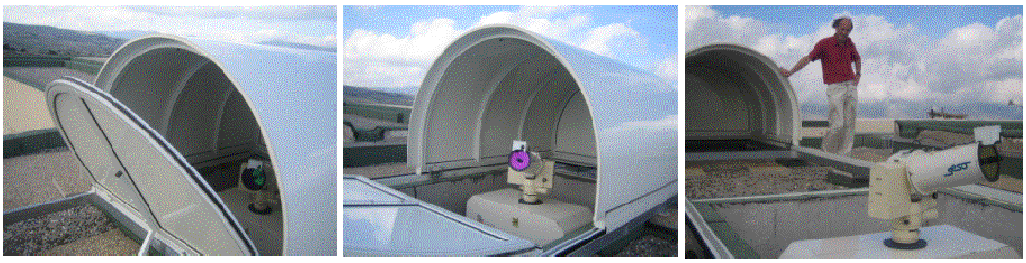

Recursive Filter Algorithm for Noise Reduction in SLR

Michael Hiener[1], Ulrich Schreiber[1], Nikolaus Brandl[2]

1. Forschungseinrichtung Satellitengeodäsie, Technical University of Munich, Fundamentalstation Wettzell, 93444 Bad Kötzting, Germany

2. Bundesamt für Kartographie und Geodäsie, Fundamentalstation Wettzell, 93444 Bad Kötzting, Germany

Contact: schreiber@fs.wettzell.de

Abstract

This report presents the concept and implementation of a recursive filter for the identification of satellite returns in laser ranging in the presence of strong noise. This project was aiming for an increased data yield of automatically filtered satellite laser ranging measurements in order to maximize the number of correctly identified returns. Furthermore the amount of false readings have to be reduced and an automatic timebias-adjustment during ranging was required.

Introduction

Automatic data screening of timer readouts in SLR is widely used by many laser ranging facilities of the ILRS. All of them depend on some type of histogram evaluation of short time slices of measurements throughout the ranging process. The approach uses the fact that return signals from a satellite bunch up at a specific location in the range gate window, while noise readouts caused by background light or intrinsic detector noise are far more spread out throughout the range gate. For satellite passes with reasonable or good signal to noise ratio this method is fully adequate. However, in particular for daylight passes of the GPS and GIOVE satellites, this method is often extracting much fewer returns than actually were recorded by the ranging facility. On top of that a non negligible number of false readings is usually upsetting the normal point generation process, because erratic data points prevent the fitting procedure from converging. Figure 1 shows an example of such a weak satellite pass. One can clearly see time intervals where a reasonable or good signal to noise ratio exists for the measurement. However there are also times where only sparse data is recorded. In order to extract the valid returns out of all the recorded data points in near real-time the control software examines small portions of the pass of a few seconds length. The data is then converted to a histogram and if a suitable bin contains a sufficient number of echoes, these are extracted and stored away as satellite returns. This evaluation process is fast and strictly linear in time. In the presence of very sparse data the threshold criterion is never satisfied and valid data is lost. If on the other side the threshold value is lowered too far, then randomly lumped together background noise events will accidentally be taken as good data and the post-processing can be disrupted.

By using more than one criterion at a time and introducing reprocessing of past data as well as a locally linearized look ahead strategy, one can vastly improve the robustness of the filter procedure. At the same time the data yield improves substantially in particular for passes with a low signal to noise ratio.

Function of the new filter algorithm

The new filter applies two distinctly different methods. A histogram-analysis is used to detect possible satellite returns in a reasonably short time interval. The results then are used to predict the likelihood of valid returns into the future, where it also

successfully recovers valid data-points at a low data rate. Both methods cooperate to not only detect, but also rate identified returns during the ranging activity.

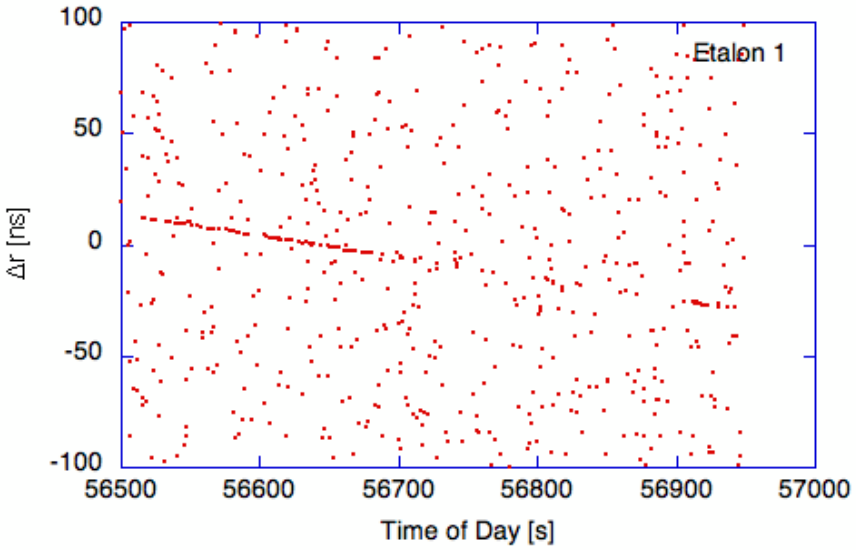

Figure 1: *Example for a measurement window of an ETALON pass with sparse data in daylight.*

From a number of verified satellite returns within a number of time slices, the actually applied time bias value for the momentarily observed satellite pass can be improved. With time bias corrected range residuals the histogram of the analysis process sharpens substantially. As a consequence the width of the rangegate can then be reduced automatically, which in turn enhances the data yield of the ranging operation. The program module works in several layers. The inner loop of the filter procedure is based on time slices of 5 seconds of observations (fig. 2). The length of the time slice is adjusted to the 10 Hz repetition rate and the background noise level typical for the Wettzell Laser Ranging System (WLRS). Other systems will have different settings. If already available a time bias correction is applied to all the data points in that time segment. Then the data is passed on to a histogram analysis routine, which has a bin width of 5 ns. This arbitrarily chosen value too has shown to work well for the WLRS operation parameters.

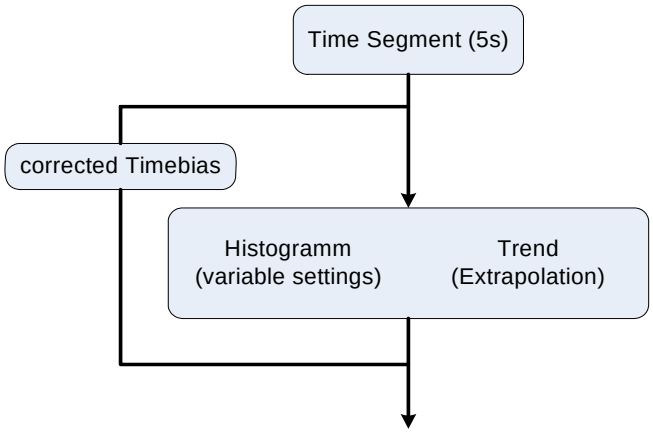

Figure 2: *Flowchart of the inner loop of the data-screening program.*

The threshold value for the histogram evaluation is currently set to 4 events per bin. In order to avoid ambiguities from unfavorable bin boundary settings (see fig. 3) in the histogram analysis, this evaluation is made twice with all the bins shifted to one side by half the bin-width.

When the threshold value of 4 events per bin is exceeded, all data points within that histogram bin are taken as possible returns. If the threshold value is exceeded by a factor of 2 the data within this bin is considered as reliably identified returns. Reliable returns are used twofold for the remainder of the satellite pass. They are used for an updated time bias computation, which feeds back to the next time slice and they are used in order to predict future locations within the range gate for the next few time slices. Figure 5 illustrates the prediction approach. Known trustworthy returns from the most recent past are linked with a straight line. The line is extended into the future and a corridor of ±2.5ns is set around this predicted line. Any single event that happens to fall within this corridor is considered a potential return and subjects it to further verification.

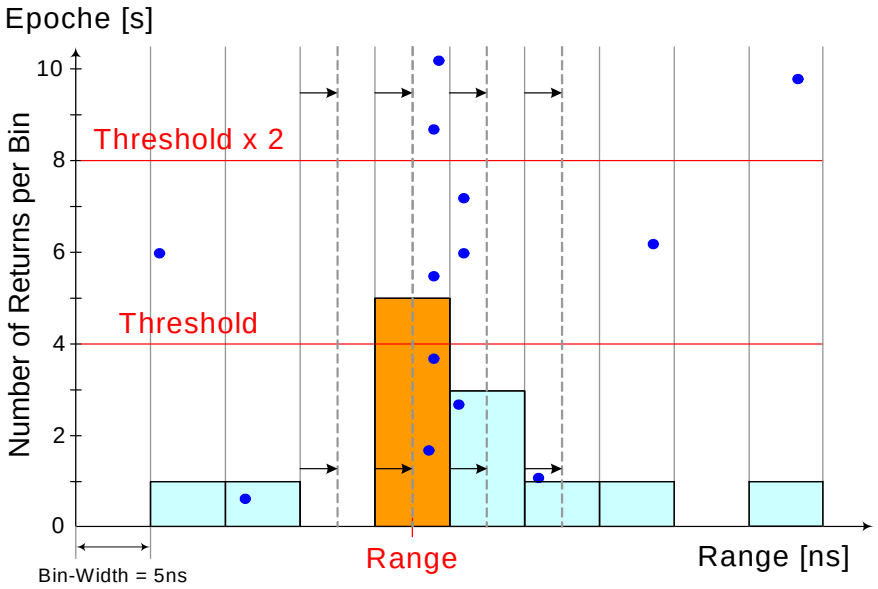

Figure 3: *A histogram of a 5 second long segment of a satellite pass of the WLRS. Unfavorable bin boundary settings are avoided by a re-evaluation with shifted bins.*

Therefore also extremely low return rates well short of the threshold value of 4 can be detected. The predicted linear corridor where future returns are expected expires after about 30 seconds when no further satellite echoes are recorded, because this simplified piecewise linearization of a satellite pass does not represent a valid approximation indefinitely.

Another important aspect of this new approach is a retrospective analysis, which identifies satellite returns that have been overlooked in the near real-time evaluation. A very sparse return rate may cause such lost returns as well as a number of false alarms. The retrospective analysis step revisits the last whole minute of observation. From the time slice analysis a number of returns are found. Some of them will be unambiguously identified as valid returns, while a certain number of returns are only classified as possible candidates. Again a linear regression through all unambiguously identified data points along with a corridor of ±2.5ns selects the part of the range gate where returns are most likely. Three cases may be found:

- All candidates (orange points in fig. 5) within these limits are now recognized as valid returns.
- All candidates outside this corridor are deleted from the list of possible returns.
- All not identified (white) data points inside the corridor are added to the list as possible candidates.

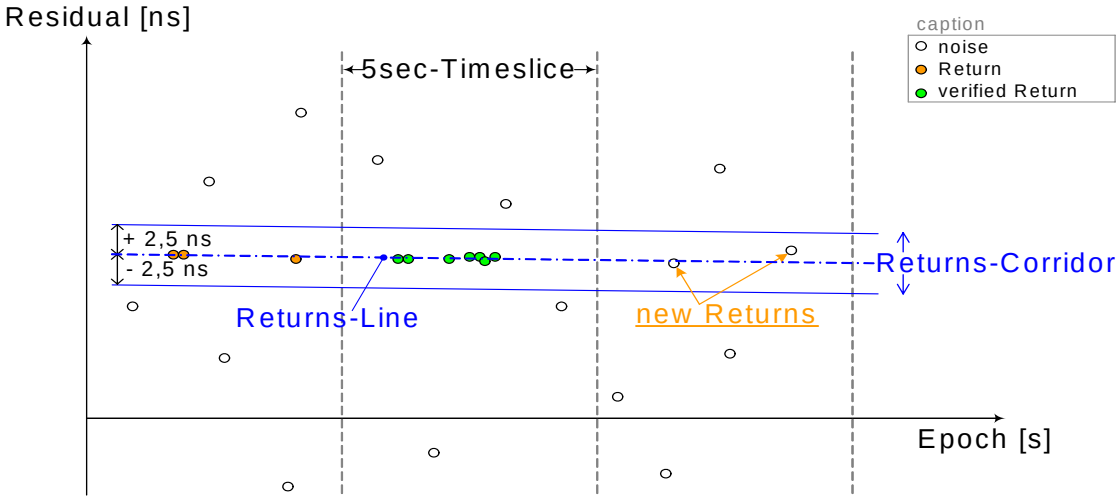

Figure 4*: *Reliably identified returns within a time slice of data are extrapolated into the future in order to find otherwise lost data points when the return rate is sparse.

The linear approach for this screening procedure is justified because only very small segments of a complete pass are analyzed at a time. It has the advantage that this processing is fast and that it does not diverge quickly as polynomials tend to do in the presence of an inhomogeneous data distribution.

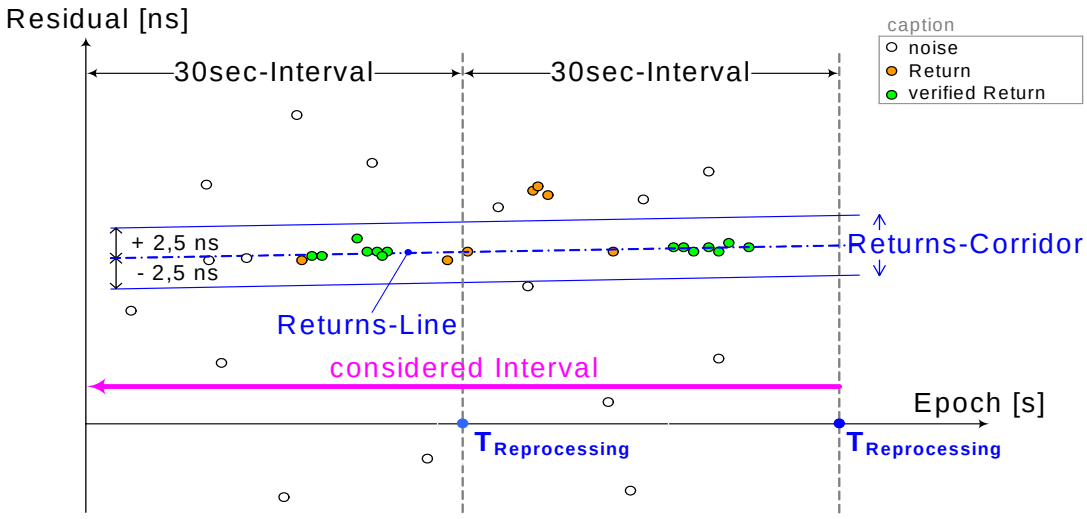

Figure 5*: *Reprocessing of the last 60 seconds of data. Reliably identified returns are used to define a return corridor. Potential returns outside this corridor are deleted from the list, while potential returns inside the corridor are turned into verified returns.

Application Results

When this new data screening approach was integrated into the routine operation software of the WLRS, care was taken that rapid data processing was maintained throughout the ranging operation. We never encountered a situation where the ranging data came in faster than the various processing steps took to evaluate the data. We would expect that this would also apply for higher repetition rate systems, however with an appropriately adapted parameter setting.

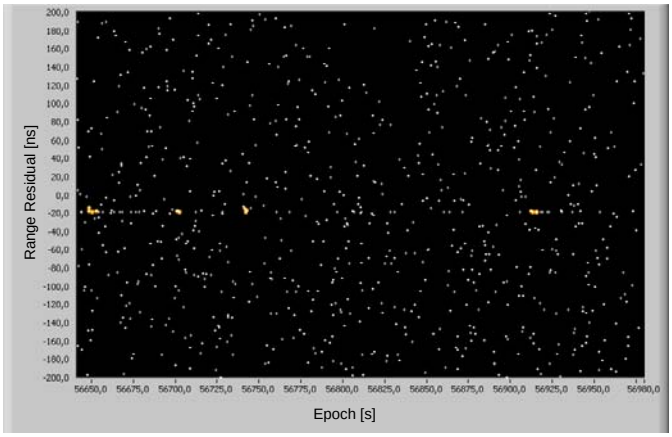

Figure 6*: A Section of an Etalon daylight pass with sparse data with returns identified with the previous screening program. Clearly many valid data points were lost in the past.*

Because of the repeated scanning of recent tracking data some adjustments to the data storage strategy had to be newly introduced. Essentially a larger data buffer is required as a temporal additional storage. As one might expect there is little to no advantage of this recursive screening filter over the simple histogram analysis when there are many satellite returns and almost no noise events. However for a weak signal to noise ratio approaching 1, rather dramatic improvements have been obtained. Figure 6 shows such an Etalon pass. Unfortunate boundary locations of the time slices often cause histograms to remain below the threshold limit. As a consequence a lot of data is lost. In this example only 12 returns were recovered out of the portion of data shown in the diagram.

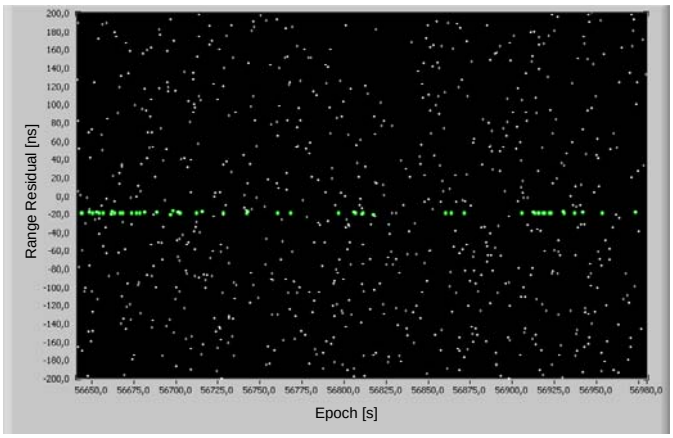

Figure 7: *The same section of the Etalon pass processed with the new screening programme.*

In contrast to fig. 6 the same dataset was re-analyzed with the new screening procedure extracting 50 returns instead of 12. The results are shown in fig. 7. Again this may still not catch all available returns. On the other hand it does not generate false readings either which is also an important aspect for this filter process. The WLRS ranging software was updated to this new filter scheme in December 2006. As far as we can see it improved the efficiency of the WLRS and reduced the number of passes that need manual user intervention for the normal point generation process noticeably.

References

[1] R. Jamal und Herbert Pichlik; LabVIEW Programmiersprache der 4. Generation; Prentice Hall, ISBN 3-8272-589-0, (1999)

[2] M. Chugani, A. Samant, M. Cerna; LabVIEW Signal Processing}; Prentice Hall PTR, ISBN 0-13-972449-4, (www.phptr.com), (1998)

The Impact and Resolution of "Collision Bands" on Tracking Targets at Various Ranges

C.J. Moore[1]

1. EOS Space Systems Pty. Limited, 111 Canberra Ave., Griffith, A.C.T. Australia.

Contact: cmoore@eos-aus.com

Abstract

Symmetric SLR and LLR systems that adopt a spinning disk as an optical switch between transmit and receive laser pulses need to address the problem of losing signal due to transmit and receive pulses being coincident at the disk when targets are at certain "collision band" ranges. These collision bands occur with increasing frequency at larger target ranges and can interrupt tracking of distant targets (> 6,000 km) for significant periods. A general solution to minimize the impact of collision bands based on disk frequency adjustment is presented. Depending on the design of the disk and system requirements, it is possible to eliminate the effect entirely or reduce the impact to a few narrow range bands by applying a relatively simple disk frequency control algorithm.

Introduction

Satellite Laser Ranging (SLR) stations that employ a symmetric (i.e. single telescope) system for their transmit and receive paths must adopt a multiplexing mechanism to allow measurement of the timing of the transmitted and received laser pulses. One popular mechanism involves the use of spinning mirrored disk containing one (or more) small holes that allow passage of the transmit pulse, while the mirrored surface is orientated such that return photons are reflected towards a receive detector. This mechanism has been adopted in recent years by EOS Space Systems for a number of their laser tracking system, including the Mt Stromlo SLR system.

One disadvantage of this mechanism is termed the "collision band" problem where a tracking signal is lost due to coincidence of a transmit hole and returning photons. The collision band thus refers to the band of target ranges that are effectively unmeasurable due to this coincidence. To increase the transmit power it can be advantageous to increase the number of transmit holes, which for a given disk rotation frequency, allows a greater laser fire rate. Unfortunately the greater the number of transmit holes, the greater the number of collision bands that may be experienced with potential loss of signal.

One technique used to minimize of collision bands relies on adjustment of the disk frequency and thus laser fire rate. For example, Titterton (1998) describes this technique to minimize backscatter. This paper describes an analysis of this collision band problem and proposes a technique for the automatic minimization of collision bands and number of disk frequency adjustments for a given range of disk configurations.

Theory

Collision Band Model

Spinning transmit/receive (T/R) disks often have one or two transmit holes, but in general there could be any number subject only to physical restrictions. Figure 1 shows a schematic of such a disk having two transmit holes. In general we can let; **N** = number of holes equally spaced around the disk, **r** = radius of the transmit hole, **R** = radius of 'projected' circle containing the transmit hole centre at fire time, and **f** = disk speed (Hz), giving the laser fire rate as **Nf**. Also let $\boldsymbol{\alpha}$ = angle subtended by each transmit hole such that $\boldsymbol{\alpha} = 2 \sin^{-1} (\mathbf{r}/\mathbf{R})$.

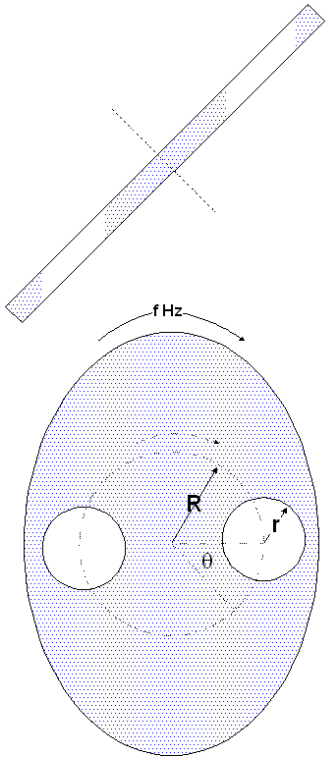

Figure 1: *Schematic of theSpinning T/R Disk*

s = available signal as a ratio, i.e. **s** = 1 when there is no loss and outgoing and incoming signals do not overlap, or **s** = 0 when complete overlap occurs.
d = distance of the target (along the optical path), and **c** = speed of light, such that the two-way time taken for a reflected pulse to leave and return to the disk is **τ = 2d/c**.
Let **θ** = angular displacement on the 'projected' circle. Given the rotation speed of a point on this circle is **2πf**, then the disk rotational movement, **Δθ,** in the time it takes for a laser pulse to leave and to return, **Δθ = 2πfτ,** is limited to

$$\frac{2\pi\, i}{N} - s\alpha < \Delta\theta < \frac{2\pi\, i}{N} + s\alpha$$

Here **i** is an integer, equivalent to the number of shots in flight.

Assume that **α** = 2**r**/**R** to a good approximation and define a geometrical factor, **F** = **sr**/**R**. This equation can be then be rewritten to give the condition for the existence of a collision band, i.e.,

$$\frac{i}{N} - \frac{F}{\pi} < f\tau < \frac{i}{N} + \frac{F}{\pi}$$

which can be expressed simply as,

$$\left| f\tau - \frac{i}{N} \right| < \frac{F}{\pi} \tag{1}$$

The number of pulses in flight, **i**, can be determined from $i = \lceil Nf\tau \rceil$, but it is wise to confirm the inequality using "floor" and "ceiling"values; i.e. $i = \lfloor Nf\tau \rfloor$ and $i = \lceil Nf\tau \rceil$.

Frequency Shifting

Equation (1) indicates that for a given range, **d**, and a given geometrical configuration there is only one parameter that can be adjusted such that the inequality no longer holds and that is the disk frequency, **f**. Hence it may be possible to adopt a scheme where the effect of collision bands can be reduced, or even eliminated, by frequency shifting the spinning disk.

From equation (1) it can be shown that to avoid a collision band at a given range, **d** (or equivalently, **τ**) then set **f** such that

$$\left| Nf\tau - \lceil Nf\tau \rceil \right| \geq \frac{NF}{\pi} \tag{2}$$

There may be additional system restrictions on the spinning disk frequency, the range of frequency adjustments that can be made and on the rate that adjustments can be made. The restrictions may be such that condition set by equation (2) cannot be met and the collision band cannot be avoided.

The next section describes an analysis of a typical two hole disk used in a laser tracking system and the scheme used to meet, as much as possible, the collision band avoidance condition given by equation (2).

Analysis of a Two Hole T/R Disk

Consider a two-hole disk having a geometrical factor F of 20%. For example, a disk where the transmit holes have a radius (projected at right angles to the laser beam) of 15 mm, at a radius from disk centre of 75 mm, or a disk with transmit holes of radius 12 mm at a distance of 60 mm from the disk centre will have F = 20% assuming no overlap of the return beam footprint on the transmit holes (s = 1.0). For this analysis assume that the maximum laser fire rate is 100Hz and the maximum frequency variation is ±5%. This is just one example of possible design constraints that might apply to systems using this technique. In this case, the value of **f** is limited to a range between 45 and 50 Hz

Table1: *Defined Range Bands*

Range Band	Sample Ranges (km)
Low Earth Orbit (LEO)	500 – 2000 km
Medium Earth Orbit (MEO)	2000 – 12000 km
High Earth Orbit (HEO)	19000 – 29000 km
Lunar	350000 – 400000 km

Table 1 summarises the four range intervals used in this analysis. These represent the typical distribution of earth orbit satellite and lunar targets. Equation (1) was applied to range values in each of these intervals to identify the collision bands occurring over the various ranges. The following sections describe the results from these calculations. In all cases the disk frequency resolution used was 0.05 Hz.

Impact of Tracking LEO Satellites

No collision bands are evident for low earth orbit ranges less than about 1,300 km as shown in figure 2. Unfortunately a collision band occurs for ranges from approximately 1450 km to 1700 km which cannot be avoided using the available disk frequency shift.

An assessment has to be made whether this collision band will cause significant impact on actual target tracking.

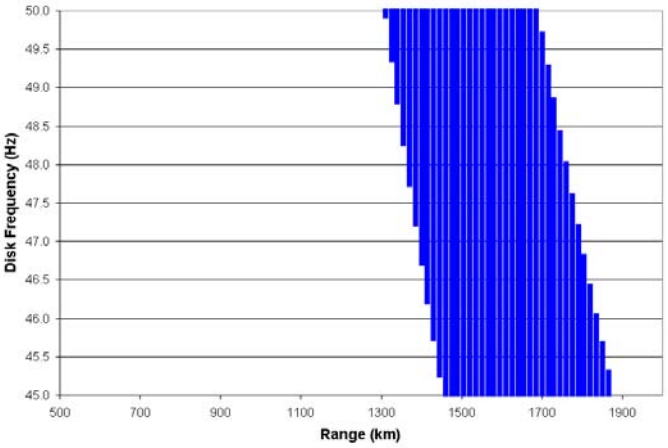

Figure 2*: Collision Bands at LEO Satellite Ranges*

Impact on Tracking MEO Satellites

For ranges between 2,000 and 12,000 km, the collision bands are grouped as shown in figure 3. There are also significant range intervals where there are no collision bands at all. However there is still one range interval where there is an unavoidable collision band, at about 3,000 to 3,200 km. Above this interval there are no ranges that have an unavoidable collision band, as illustrated in figures 3, 4 and 5.

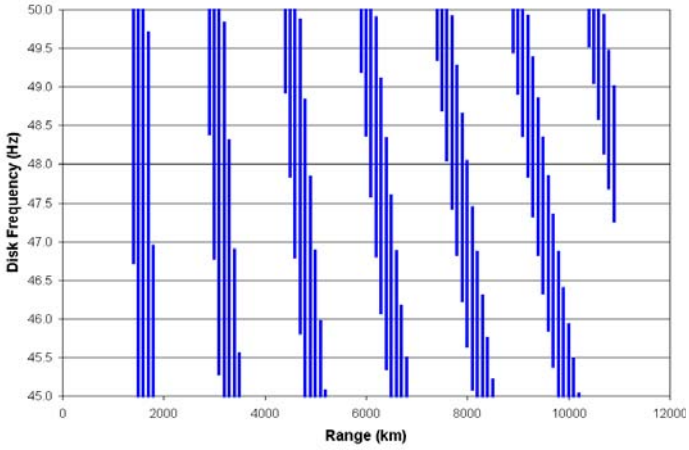

Figure 3*: Collision Bands at MEO Satellite Ranges*

Impact on Tracking HEO Satellites

As ranges increase, the number of collision bands within the disk frequency range increase and become shorter, as illustrated in figures 4 and 5, so the options for avoiding collision bands also increases. However, for any given disk frequency, the probability of a target pass having a number of collision bands also increases.

It is notable that even for one-hole disk systems, the probability that a high satellite pass contains one or more collision bands is quite high, and hence an avoidance scheme is still required.

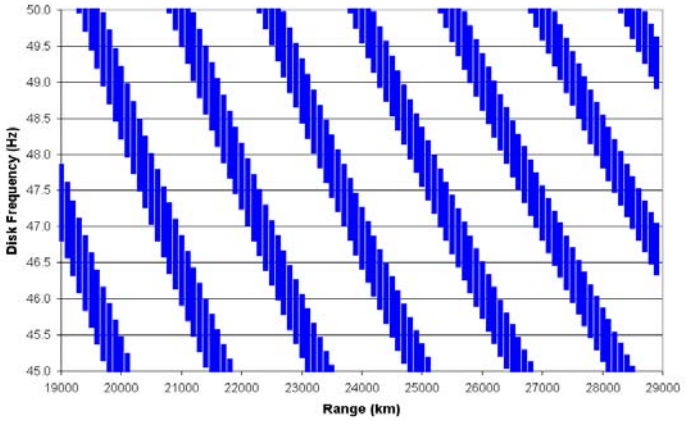

***Figure 4**: Collision Bands at HEO Satellite Ranges*

Impact on Tracking Lunar Targets

At lunar target distances, collision bands are very frequent but very short both in terms of disk frequency and range changes as illustrated in figure 5. With slowly changing ranges, it is possible that a lunar target pass may either be largely free of collision bands or be largely in a collision band. Avoidance at these ranges will require small shifts in disk frequency. Table 2 shows a summary of typical impact of collision bands on tracking a number of ILRS SLR satellites and LLR targets.

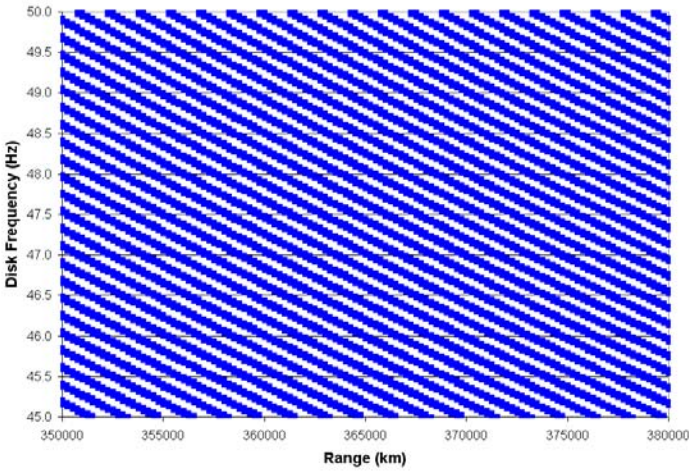

***Figure 5**: Collision Bands at Lunar Ranges*

***Table 2**: Impact of Collision Bands on ILRS Satellites*

Satellite Groups	Typical Ranges (km)	Impact, no avoidance	Impact with avoidance
GraceA & B, Champ	500 – 1500	None	None
Envisat, ERS2, GFO1, Stella, Starlette	800 – 2000	Lost data around 1500-1700 km (near end of passes)	Lost data around 1500-1700 km (near end of passes).
Ajisai, Jason	1400 – 2900	Lost data near zenith of high passes.	Lost data near zenith of high passes.
Lageos1,2	5900 – 9,000	Lost data in 1 or 2 bands.	None
GPS, Etalon, Giove A, Galileo	19,000 – 27,000	Lost data in 2 or 3 bands.	None
LLR targets	350000 – 420,000	Significant periods of lost data	None

Collision Band Avoidance

Frequency Shifting Algorithm

Using equation (1) it is straightforward to assess, given current range and disk frequency, whether a tracking system is experiencing a collision band. However it is less straightforward to determine what is the best disk frequency to use to avoid such a band. An algorithm was devised such that not only are collision bands avoided (if at all possible) but the number of

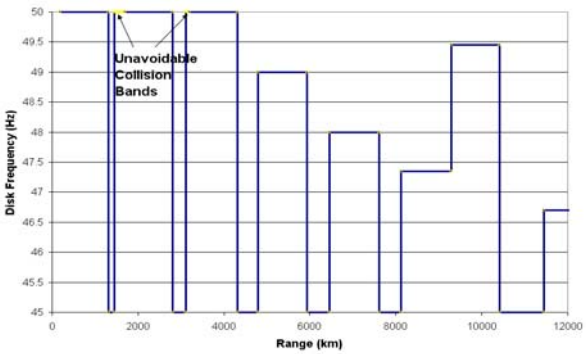

***Figure 6**: Disk Frequency over increasing LEO and MEO Satellite Ranges*

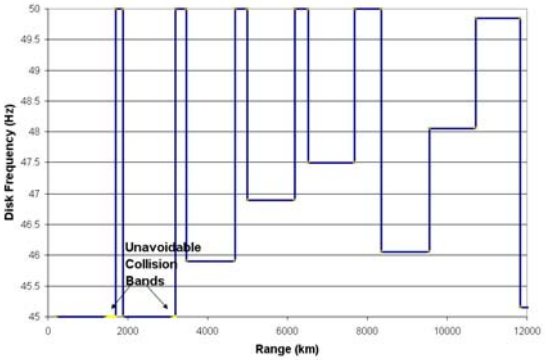

***Figure 7**: Disk Frequency over decreasing LEO and MEO Satellite Ranges*

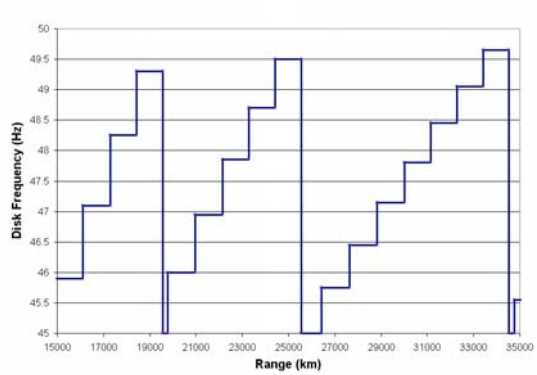

***Figure 8**: Disk Frequency over increasing HEO Satellite Ranges*

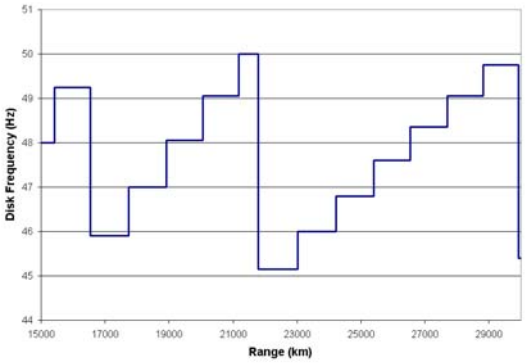

***Figure 9**: Disk Frequency over decreasing HEO Satellite Ranges*

frequency adjustments is minimized. This may be important if the time taken for the laser system to respond to frequency changes is significant.

The algorithm requires determining, for a given range, the disk frequency end points of a given collision band, at the moment that this collision band is first encountered. No action (i.e. frequency adjustment) is necessary when a collision band is not present. If a collision band is encountered when the range is increasing, increase the disk frequency by a small amount and check if the collision band is still present. This is repeated until maximum disk frequency is reached, at which point, the disk frequency is set to the minimum, and then adjusted upwards until no collision band is found or the cycle is completed and avoidance is not possible. A similar procedure is followed when the range is decreasing but in this case the disk frequency is reduced by a small amount.

The following diagrams illustrates the disk frequency changes (for the sample configuration) resulting from the application of this algorithm. Results from increasing and decreasing

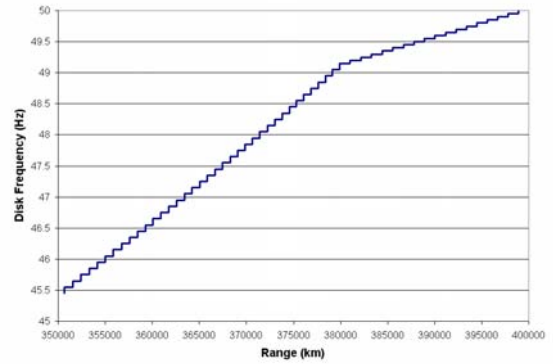

***Figure 10**: Disk Frequency over increasing Lunar Target Ranges*

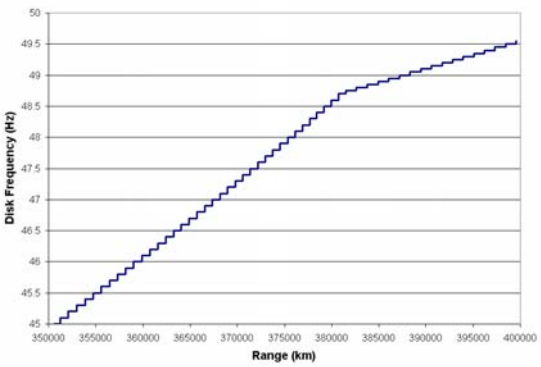

***Figure 11**: Disk Frequency over decreasing Lunar Target Ranges*

ranges are shown.

Low-Medium Earth Orbit Satellite Ranges

The frequency shift patterns for increasing and decreasing distances over the low and medium earth orbit satellite ranges are shown in the figures 6 and 7. Note there are two small ranges where collision bands are unavoidable by frequency shifting for the two hole configuration used.

High Earth Orbit Satellite Ranges

The frequency shift patterns for increasing and decreasing distances over the high earth orbit satellite ranges is shown in the figures 8 and 9. There are no unavoidable collision bands.

Lunar Target Ranges

The frequency shift patterns for increasing and decreasing distances over lunar target ranges is shown in figures 10 and 11. There are no unavoidable collision bands.

Disk Design

Given a geometrical design of the disk, the disk rotation frequency can be used to minimize collision bands as described in the previous section. However can the need for frequency shifting be ameliorated by appropriate disk geometry? The number of transmit holes and the

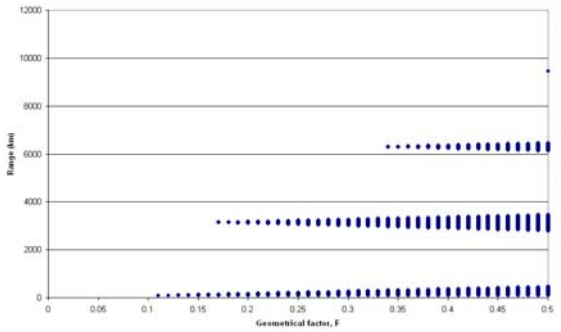

Figure 12: *Unavoidable bands for a 1 hole disk.*

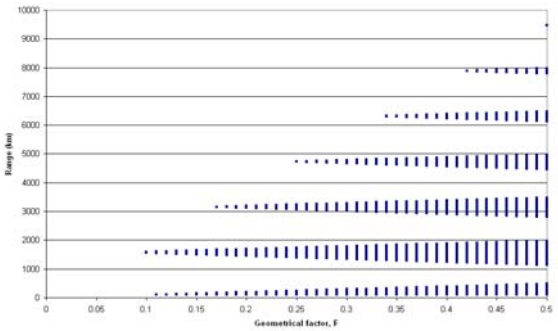

Figure 13: *Unavoidable bands for a 2 hole disk.*

geometrical factor, F, will influence the occurrence of collision bands and this is illustrated in Figure 12 for a 1 hole disk and Figure 13 for a 2 hole disk operating between 45 and 50Hz as in the previous examples. Similar diagrams can be generated for disks having three or more holes. These diagrams show the ***unavoidable*** collision bands at various ranges and various F-factors.

Clearly, more holes will result in a greater number and width of unavoidable bands over ranges up to 8,000 km. However, if the T/R disk and associated transmit hole can be designed such that $F < 0.1$ then the performance of disks with multiple holes (at least up to 3) is greatly improved. If the transmit hole radius had to be greater than, say, 10 mm, to accommodate the laser beam, then to obtain $F = 0.1$, the centre of the transmit hole would have to be greater than 100 mm from the centre of the T/R disk. Whether this is achievable would depend on other design criteria.

References:

[1] Titterton, P., "System/Usage Impact of Operating the SLR2000 at 2 Khz,". Proceedings of the 11th International Workshop on Laser Ranging, 1998, Deggendorf.

Web Application for the Engineering Data Files Processing

K.Salminsh

1. Institute of Astronomy, University of Latvia.

Contact: kalvis@lanet.lv /Fax: +371 7034582

Abstract

One of the problems of introducing new data formats and procedures is a high cost in terms of manpower and time to develop, modify and deploy necessary software across the SLR network. Web applications are a relatively new type of applications located on the server and accessible via the web browsers hence simplifying the software distribution and making any changes and improvements immediately accessible to all users. In this report the web application for the Engineering Data Files (EDF) processing and analysis is considered in more details. Review of the existing functionality and future development is presented.

Introduction

As was shown in [1] the preferable way to handle Engineering Data Files (EDF) processing and analysis is a web application to reduce overall implementation costs accross the ILRS network and to make software and its eventual future changes immediately accessible to the all users. For more detailed information on the EDF's, see [2]. Another advantage of the web applications is their accessibility to everyone with an internet connection and web browser (security restrictions may apply).

EDF Processing Application

Overview of the current implementation of the EDF processing workflow is presented in [2]. Incoming EDF from stations are uploaded via FTP and after preprocessing are moved to the directories for anonymous ftp access and also are inserted in the relational database. Data then can be accessed and processed over the Internet using the dedicated web application. Web application basic functionality, based on the goals stated in [1], can be summarized as following:

- Overview of the used equipment
- Calibration time series and analysis
- Calibration charts
- External interfaces: data export to Excel, web feeds (e.g. RSS)

The use of the application is straightforward. The equipment overview function (Figure 2) allows users to retrieve data about the equipment used in a given period of time for all stations, and to use it as a selection criteria for the calibration time series and to calculate statistics for one or more stations. The selected data can then be compared, plotted or exported to an Excel spreadsheet and downloaded to the user computer. Tabular data view for the Excel export is presented in the Figure 3. Live calibration data can be also published from the database as an RSS feed directly usable in other applications or web sites.

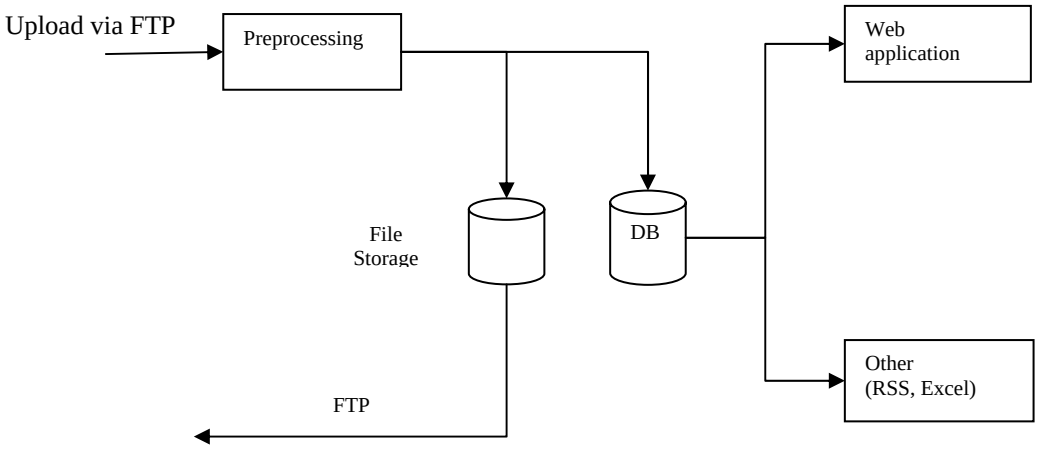

***Figure 1**: EDF processing flow*

Implementation details and future extensions

The EDF processing web application is now deployed on the server at the Institute of Astronomy, Institute of Latvia, and access information will be published on the EDF website [2]. The application is running on a Windows 2003 server and using a Firebird 1.5 relational database for the data storage. The most challenging part of the application is calibration data selection based on the used hardware and data model in the database. This is because it involves optional and station specific data within EDF XML documents and it leads directly to tree data structures which don't map well into the relational database structure. The current solution is to make directly accessible within the database only required parameters from the EDF specification, and to limit the number of parameters available for the data selection. The list of key parameters currently made available for data search and selection are:

- Station
- Calibration epoch
- Detector type
- Timer type
- Laser

Another limitation of the current design and data model is that the station custom data recorded within EDF can be used only as a reference and should be retrieved from the original EDF and stored in the database table as an entity, separately. Hence one of possible future extensions may include migration to the XML database to remove these limitations. Other eventual improvements are related to the user interface and application functionality including improvements in the data model.

Conclusions

One of the main problems in designing the EDF processing application is the absence of a common naming standard for the SLR station basic hardware elements and their parameters which can have an adverse impact on obtaining ranging results. Very likely similar problems will be encountered by others trying to record, process and analyze SLR data.

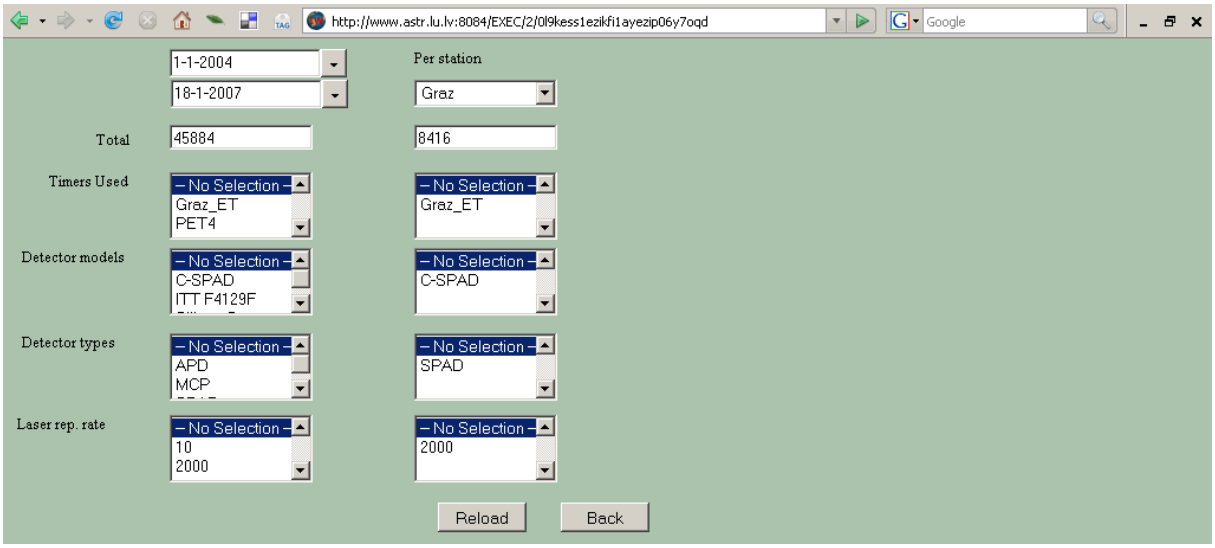

Figure 2: *Hardware overview and selection*

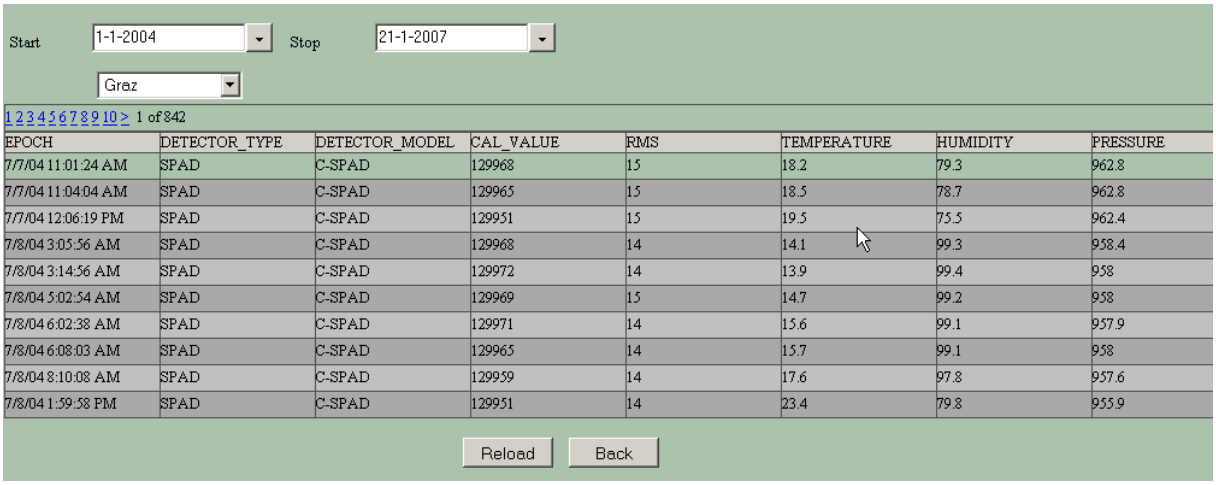

EPOCH	DETECTOR_TYPE	DETECTOR_MODEL	CAL_VALUE	RMS	TEMPERATURE	HUMIDITY	PRESSURE
7/7/04 11:01:24 AM	SPAD	C-SPAD	129968	15	18.2	79.3	962.8
7/7/04 11:04:04 AM	SPAD	C-SPAD	129965	15	18.5	78.7	962.8
7/7/04 12:06:19 PM	SPAD	C-SPAD	129951	15	19.5	75.5	962.4
7/8/04 3:05:56 AM	SPAD	C-SPAD	129968	14	14.1	99.3	958.4
7/8/04 3:14:56 AM	SPAD	C-SPAD	129972	14	13.9	99.4	958
7/8/04 5:02:54 AM	SPAD	C-SPAD	129969	15	14.7	99.2	958
7/8/04 6:02:38 AM	SPAD	C-SPAD	129971	14	15.6	99.1	957.9
7/8/04 6:08:03 AM	SPAD	C-SPAD	129965	14	15.7	99.1	958
7/8/04 8:10:08 AM	SPAD	C-SPAD	129959	14	17.6	97.8	957.6
7/8/04 1:59:58 PM	SPAD	C-SPAD	129951	14	23.4	79.8	955.9

Figure 3*: Calibration time series – table view*

References

[1] Salminsh K. “Engineering Data File Processing and Distribution”, p.377, 14th International Laser Ranging Proceedings, San Fernando 2004.

[2] Website: http://www.astr.lu.lv/EDF

Consolidated Laser Prediction and Data Formats: Supporting New Technology

R. Ricklefs[1]

1. Center for Space Research,The University of Texas at Austin.

Contact: ricklefs@csr.utexas.edu for the ILRS Prediction Format Study Group and the Data Formats and Procedures Working Group

Abstract

The new tabular ILRS Consolidated Prediction Format (CPF) was developed to provide a single format to encompass traditional artificial satellite and lunar ranging targets as well as proposed transponder targets on or around the moon and other planets. As implementation of this format nears completion, the need to effectively handle kilohertz firing rates and transponder data in a new data format has emerged. The proposed Consolidated Laser Ranging Data Format (CRD) carries with it the lessons learned from the CPF: modularity, flexibility, and expandability.

Introduction

At the International Laser Ranging Service (ILRS) Workshop in Matera, Italy in 2000, it was decided that a new prediction format was needed to encompass the existing satellite and lunar ranging targets as well as the often-discussed transponders. In addition, there was a need to improve the predictions for low earth satellites. Thus the consolidated prediction format (CPF) was developed as a single format for all laser ranging targets, present and future. As the process of implementing the CPF is winding down, technological changes, in particular kilohertz repetition rate lasers and the Lunar Reconnaissance Orbiter (LRO) transponder are demanding that the current laser data formats be similarly reformulated. The process of creating the Consolidated Laser Ranging Data Format (CRD) is moving forward to meet LRO mission deadlines.

Consolidated Prediction Format

As described in early documents (Ricklefs, 2004, 2006), the CPF provides a method of ranging to different types of targets using one format. It therefore allows cross-technique ranging attempts, provided that a ranging station has needed hardware capabilities – such as event timers for lunar ranging.

The CPF does not rely on the on-site gravity model, tuning, separate Earth Orientation series, or drag and time bias functions that were required for the older tuned inter-range-vector (TIV) system. Instead, the new format contains untuned state vectors at appropriate intervals, typically in the ITRF system. This so-called format change is actually a change to the entire prediction scheme at the laser station from one of integration to one of interpolation.

Consolidated Prediction Format: Implementation Status

Currently (as of late October, 2006), the CPF is used exclusively in at least 22 out of the 37 ILRS Satellite Laser Ranging (SLR) stations, with one station in late stages of testing and 5 others close behind. Many of the remaining stations are not currently operational. It is expected that all operational stations will be converted by early 2007. In addition, the format is used at the one currently operating Lunar Laser Ranging (LLR) station (McDonald Laser Ranging Station), with other stations experimenting

with the format. The author is also working with the LRO project to generate CPF files. This effort may result in some additional transponder-specific changes to the format.

The results from using the CPF seem to be quite promising. According to one station (Gibbs, 2006), SLR predictions are seen to be much more accurate, with 90% of passes being within +-20nsec and 99% being within +-100nsec of the predicted range.

Consolidated Laser Ranging Data Format: Motivation

The first concern with the existing data formats (ILRS, 1999, 2004) is that transponder data will not fit. Specifically, transponders will often need to deal with one-way ranges. For instance, LRO data will consist of a fire time on the ground and receive time at the satellite. This being the case, there is a need for more accuracy in the fire and receive times, as the difference between the two must accommodate the accuracy expected from a range, usually at the picosecond level. This highlights the third issue, that of clock information. The current time standards, such as GPS are accurate only to about 100ns. Thus, there must be a way of describing the time standard used to record the data – on both the ground station and spacecraft. This is accomplished with a time system flag, a time offset, and a drift rate for both. Calibration is yet another area needing expansion. In the same way that there are laser station system delays, there are similar system delays on the spacecraft that must be accounted for.

In addition to the demand to reshape the data formats for transponders, stations with kilohertz laser firing rates are becoming more common and must be accommodated. Among the advantages, kilohertz laser ranging offers the possibility to study a satellite's signature in more detail than ever before, providing details of the spacecraft rotation rate and corner cube performance (Arnold, et. al., 2004). The existing fullrate data format is cumbersome for use with high-repetition-rate systems, because there is so much redundant information found in each data record. Estimates for the draft version of the format show that fullrate file size should drop by 55-65% at 500 returns/sec and 25-30% at <10 returns/sec.

Consolidated Laser Ranging Data Format: Overview

The intent of the new format is to encompass full rate, sampled engineering, and normal point data in one flexible, ASCII data format. The structure will be similar to that for the Consolidate Prediction Format in that there are several types of header and data records, assembled in a building-block approach, with records capable of specifying data for a particular data type or spacecraft configuration. This makes the format extensible and flexible. An additional section, for system configuration information, is being considered. A configuration section would make the data more self-documenting with more detailed data being available to the analyst. As with the CPF, header records are fixed format, but data (and configuration) records are free format, allowing field sizes to be optimized for each satellite.

Sampled engineering, fullrate, and normal point data could be placed in one file or broken into 3 files. Multiple color data could be included in one file, as could data from one or more satellites or stations. Simple utility programs could facilitate the merging or parsing of files. The hope is to make the format XML-friendly so that the data files could be easily parsed and written into XML files, and an XML representation of the data could easily be written in the CRD format.

In the case of transponders, much of the data required to write the complete CRD file is not available at the ranging stations in real time. The data that is recorded can be transmitted to the mission data center where all the data is collated, quality controlled, and finally submitted to the ILRS data center. Normally, one would expect that the stations would create and submit partially populated CRD files which the mission data center would complete.

Timetable

The LRO mission has become a driver for creation and implementation of the new data format, since its schedule is so tight, with launch in late 2008. At some point a version of the format will need to be frozen for this mission, even if the format is not ready for network-wide implementation. (Fortunately, on-station data for LRO will be written into a compact intermediate format, so 2 versions of the CRD will not be implemented at participating stations.) The version presented here, version 0.09 will probably be used for LRO.

In the near future, the preliminary format will be made available on the ILRS web site. The general community will be invited to submit comments.When the format is finalized, its implementation will take place over a period of a year or so, with stations in most need of the new features implementing it first. These include kilohertz stations, transponders-ranging stations, and lunar stations. The lunar ranging on-station raw format has always contained data not transmitted through the ILRS formats.

There has been some concern on the part of analysts that they would find it disruptive to deal with more than one data format at a time. For this reason, the data centers will translate normal point data received in the new format into the current ILRS format until all stations are using the new format. At some time, historical data, especially normal points, will need to be translated into the new format. This may have to be phased in over a number of years, once the format has been implemented and as resources become available. This topic needs to be discussed in more depth.

Summary

The successful implementation of the new prediction format is drawing to a conclusion at the same time that new technology such as kilohertz ranging and the LRO transponder are demanding that the laser data formats be rewritten. The new data format (CRD) will encompass fullrate, sampled engineering, and normal point data for SLR, LLR, and TLR. As with the CPF, the CRD format will use a building-block approach to permit modularity, expandability and extensibility.

References

[1] Arnold, D., G. Kirchner, and F. Koidl: “Identifying Single Retro Tracks with a 2kHz SLR System – Simulations and Actual Results”, Proceeding of the Fourteenth International Workshop on Laser Ranging, San Fernando, 2004.

[2] Gibbs, P.: Private communications, 2006.

[3] ILRS: “ILRS Fullrate Format Version 3”, http://ilrs.gsfc.nasa.gov/products_formats_procedures/fullrate/fr_format_v3.html, 1999.

[4] ILRS: “ILRS Normal Point Format, Revision 2”, http://ilrs.gsfc.nasa.gov/products_formats_procedures/normal_point/np_format.html, 2004.

[5] Ricklefs, R.: “Consolidated Laser Ranging Prediction Format: Field Tests”, Proceeding of the Fourteenth International Workshop on Laser Ranging, San Fernando, Spain, 2004.

[6] Ricklefs, R.: “Consolidated Laser Ranging Prediction Format”, http://ilrs.gsfc.nasa.gov/products_formats_procedures/predictions/cpf.html. 2006.

Appendix A: New CRD Format Examples

The following data examples are based on the preliminary 0.09 version of the format and are included for demonstration purposes only. Changes being made to the format document will render these examples obsolete.

1. Headers

1.1 Basic header 1

H1 CRD 1 MLRS   2006 9 27 17 0 ENVISAT   test file

Note station and satellite names.

1.2 Basic Header 2

H2   200901 6179   27386 2003 11 11 5 31 24 2003 11 11 5 32 2 52954 7080 24 19 1 0 6 7 2 0

Note the begin and end times and modified julian date of first data record as well as numerical station and satellite IDs.

1.3 Laser color record

H4 1 532.0

One such record is included for each laser color recorded in the file.

1.4 Pass Information

H5 1   -650   0   82   82

This record contains statistical information on the data and calibrations. The final format is likely to include the often-requested skew and kurtosis of the data in addition to the RMS.

1.4 End of Header

H9

Additional headers for transponders and full rate information are not shown here. Headers are fixed format

2. Data records

2.1 Range Record

10 1 2   19880.8466929 1 2   0.010936014472   0

The first long field is the transmit time, and the second long field is either range or receive time at the spacecraft. In the case of a down-link transponder, the first log field would be the transmit time at the satellite, and the second would be the receive time at the ground station. Interpretation of these fields is controlled by flags fields.

2.2 Meteorological record

20   19880.8466929 802.50 288.10   69

This record is written at the beginning of the file and thereafter only when one of the fields change “significantly”. This could be defined as twice the least significant bit of the sensor or an amount based on the field, such as 0.02mB for atmospheric pressure.

2.3 Point angles

30   19880.8466929 1 281.1890 22.4030

Point angles would be written for sampled engineering and fullrate data. After the beginning of the data, additional record are written only when a field changes “significantly.”

2.4 Corrections

40   19880.8466929 1 2   0   0   -650   0

This record includes refraction, center of mass, and system delays. Additional records are written only when a field changes “significantly.”

2.5 Range (with normal point fields)

10 2 2   19884.7472085 1 2   0.010985288919   0   15   37   73   0.0

Note that data records are written in free format.